



# **ESA Cryosat Mission**

## **Mission Study and Reverse Engineering**

Course of Space Systems Engineering and Operations

Prof. Lavagna M.

Luca Caffiero  
Andrea D'Uva  
Luca Marchesotti  
Baptiste Romain  
Riccardo Siri  
Alessia Sollo

**A.Y. 2021/2022**

# Nomenclature

## Abbreviations

ADCS	Attitude Determination and Control Subsystem
AO	Atomic Oxygen
BOL	Beginning of Life
CCD	Charge Coupled Device
CDH	Command and Data Handling
CDMU	Command and Data Management Unit
CESS	Coarse Earth and Sun Sensor
CNES	Centre National D'études Spatiales
DoD	Depth of Discharge
DPU	Digital Processing Unit
EOL	End of Life
EPS	Electric Power Subsystem
FFT	Fast Fourier Transform
FOV	Field Of View
GS	Ground Station
IAT	International Atomic Time
IF	Intermediate Frequency
IGN	Istitut National de l'Information Geographique et Forestière
LEO	Low Earth Orbit
LEOP	Launch and Early Orbit Phase
LST	Local Solar Time
LV	Launch Vehicle
MLI	Multi Layer Insulator
OBDH	On Board Data Handling
OC	On Board Computer
PCDU	Power Conditioning and Distribution Unit
PDS	Payload Data Segment
PRF	Pulse Repetition Frequency
RAAN	Right Ascension of the Ascending node
RCS	Reaction Control Subsystem
RF	Radio Frequency
RFU	Radio Frequency Unit
SA	Solar Arrays
SAR	Synthetic Aperture Radar
SLOC	Source Line Of Code
SRP	Solar Radiation Pressure
SSO	Sun Synchronous Orbit
SSSR	Sequential Switching Shunt Regulator
SSPA	Solid-State Power Amplifier
ST	Star Tracker
TLC	Transport and Launch Canister

# Contents

<b>1 Mission Overview</b>	<b>1</b>
1.1 Mission Objectives . . . . .	1
1.1.1 Mission Rationale . . . . .	2
1.2 Functional Analysis . . . . .	2
1.2.1 High-level functionalities . . . . .	2
1.2.2 Payload Functionalities . . . . .	3
1.3 Payloads . . . . .	3
1.3.1 SIRAL . . . . .	3
1.3.2 DORIS . . . . .	7
1.3.3 LRR . . . . .	8
<b>2 Mission Analysis</b>	<b>9</b>
2.1 Orbit . . . . .	9
2.1.1 Orbit Evolution . . . . .	11
2.1.2 Orbital Maintenance and ΔV Budget . . . . .	12
2.1.3 Orbital Decay . . . . .	14
2.2 Environmental Analysis . . . . .	15
2.2.1 Debris and Micrometeors . . . . .	15
2.2.2 Magnetic Field . . . . .	16
2.2.3 Atomic Oxygen . . . . .	16
2.2.4 Radiations . . . . .	17
2.3 Mission Phases . . . . .	18
2.3.1 Launch and Early Orbit Phase . . . . .	18
2.3.2 Commissioning Phase . . . . .	18
2.3.3 Science Phase . . . . .	19
2.3.4 Disposal Phase . . . . .	19
2.3.5 Operational Modes . . . . .	19
2.3.6 Conceptual Operations - ConOps . . . . .	19
<b>3 System Analysis</b>	<b>20</b>
3.1 Telecommunication System . . . . .	20
3.1.1 Functionalities . . . . .	20
3.1.2 Space links and frequency selection . . . . .	20
3.1.3 Architecture . . . . .	21
3.1.4 Link budget analysis . . . . .	23
3.1.5 Visibility and Data download . . . . .	24
3.2 Propulsion System . . . . .	25
3.2.1 Functionalities . . . . .	25
3.2.2 System Selection . . . . .	26
3.2.3 Reaction Control System Configuration . . . . .	27
3.2.4 System Architecture . . . . .	28
3.3 Attitude Determination and Control System . . . . .	30
3.3.1 Functionalities . . . . .	30
3.3.2 System Definition . . . . .	31
3.3.3 Sensors Description . . . . .	31
3.3.4 Disturbances Analysis and Actuators Selection . . . . .	32
3.3.5 Modes . . . . .	33
3.4 Electric Power System . . . . .	34
3.4.1 Functionalities . . . . .	34

3.4.2	Power source selection . . . . .	34
3.4.3	Power budget breakdown . . . . .	35
3.4.4	Primary power source sizing - SA . . . . .	36
3.4.5	Secondary power source sizing - Battery . . . . .	38
3.4.6	Conclusions . . . . .	39
3.5	Thermal Control System . . . . .	39
3.5.1	Functionalities . . . . .	39
3.5.2	Temperature Range . . . . .	39
3.5.3	Thermal Analysis . . . . .	40
3.6	Configuration . . . . .	42
3.6.1	System Positioning . . . . .	42
3.6.2	Mass budget . . . . .	44
<b>A</b>	<b>CryoSat's Configuration</b>	<b>i</b>
<b>B</b>	<b>Launcher</b>	<b>ii</b>
<b>C</b>	<b>Engine Comparison</b>	<b>iii</b>
<b>D</b>	<b>Thermal Analysis</b>	<b>iv</b>
D.1	Results of refined MLI selection . . . . .	iv
D.2	Results of initial MLI selection . . . . .	v
<b>E</b>	<b>On-Board Data Handling</b>	<b>vi</b>
E.1	Functionalities . . . . .	vi
E.2	Baseline architecture . . . . .	vi
E.3	OC performance estimation . . . . .	vii
E.4	Hardware . . . . .	ix
<b>F</b>	<b>Requirements</b>	<b>x</b>
F.1	Mission Requirements . . . . .	x
F.2	Environmental Requirements . . . . .	x
F.3	Design Requirements . . . . .	xi
F.4	Telecommunication System . . . . .	xi
F.5	Propulsion System . . . . .	xi
F.6	Attitude Determination and Control System . . . . .	xii
F.7	Electric Power System . . . . .	xii
F.8	Thermal Control System . . . . .	xiii
F.9	On Board Data Handling . . . . .	xiii
F.10	Configuration . . . . .	xiii
<b>Bibliography</b>		<b>xiv</b>

# List of Figures

1.1	CryoSat mission's logo . . . . .	1
1.2	Payload position [1] . . . . .	3
1.3	CryoSat bottom view, artistic impression . . . . .	4
1.4	SIRAL Geographic Mode Mask, week 34, August 2019 . . . . .	5
1.5	DORIS ground station locations . . . . .	7
1.6	DORIS antenna . . . . .	7
1.7	CryoSat's Laser RetroReflector . . . . .	8
2.1	Duration of the eclipses in the first year following the launch date April 9 <sup>th</sup> 2010 . . . . .	10
2.2	Duration of the eclipses for SSO for the year starting on April 9 <sup>th</sup> 2010 . . . . .	10
2.3	Time of visibility from Kiruna of the nominal orbit . . . . .	10
2.4	Time of visibility from Kiruna of the SSO . . . . .	10
2.5	Latitude vs time on nominal orbit . . . . .	10
2.6	Latitude vs time on SSO . . . . .	10
2.7	Semimajor axis evolution . . . . .	11
2.8	Eccentricity evolution . . . . .	11
2.9	Inclination evolution . . . . .	12
2.10	Anomaly of the Pericentre evolution . . . . .	12
2.11	First ground track vs ground track after 3 full (nominal) cycles with no corrections . . . . .	12
2.12	Number of Maneuvers per Year . . . . .	14
2.13	Number of Sunspot . . . . .	14
2.14	Orbital decay reduced time vs perigee height and eccentricity[2] . . . . .	15
2.15	Numbers of acknowledged man made object in space according to ESA[3] . . . . .	15
2.16	Number of debris per type[3] . . . . .	15
2.17	Mass flux of debris and micrometeors on CryoSat's orbit . . . . .	16
2.18	Intensity of Earth's magnetic field experienced over (approximately) 24 hours of orbit . . . . .	16
2.19	Intensity of Earth's magnetic field vs satellite's location . . . . .	16
2.20	Atomic Oxygen flux . . . . .	17
2.21	Protons trapped flux . . . . .	17
2.22	Electrons trapped flux . . . . .	17
2.23	Fluence of trapped particles for the thirteen years of orbit . . . . .	18
2.24	Protons trapped flux of cosmic origin . . . . .	18
2.25	Conceptual Operations of the CryoSat Mission . . . . .	19
3.3	Simulated downloaded data per day from 10 <sup>th</sup> April 2010 to 8 <sup>th</sup> May 2010 compared to the real data . . . . .	25
3.4	Comparison of the specific impulses for the most common operating gases. . . . .	27
3.5	Accommodation of the attitude/orbit control thrusters. (ACT/OCT) . . . . .	28
3.6	Propulsion System Schematic . . . . .	28
3.7	Mass and external radius ratio between cylindrical and spherical tanks vs slenderness ratio for the same internal volume. . . . .	29
3.8	Pressure ratio along the axis of the OCT nozzle . . . . .	30
3.9	Sum of Environment disturbance torques in body axes . . . . .	32
3.10	Required moment dipole to compensate the disturbances . . . . .	33
3.11	ADCS control logic scheme . . . . .	34
3.12	Power source alternatives and taxonomy . . . . .	35
3.13	Multinodal Model and Cases . . . . .	40
3.14	Equivalent thermal circuit. . . . .	40
3.15	CryoSat internal view of its systems elements [1] . . . . .	43

---

3.16 CryoSat internal view of its payload and ST [1] . . . . .	43
3.17 Cryosat configuration, internal view . . . . .	44
A.1 CryoSat's dimensions . . . . .	i
A.2 CryoSat inside the fairing . . . . .	i
B.1 Launcher Con-ops . . . . .	ii
C.1 Apocentre radius variation. . . . .	iii
C.2 Propellant mass consumption. . . . .	iii
D.1 Hot case 1: Sun direction along y-axis. . . . .	iv
D.2 Hot case 2: Sun direction along z-axis . . . . .	iv
D.3 Hot case 3: Sun direction normal to the SA . . . . .	iv
D.4 Cold case: Eclipse . . . . .	iv
D.5 Dynamic Thermal Study . . . . .	iv
D.6 Hot case 1 (general MLI): Sun direction along y-axis. . . . .	v
D.7 Hot case 2 (general MLI): Sun direction along z-axis . . . . .	v
D.8 Hot case 3 (general MLI): Sun direction normal to the SA . . . . .	v
D.9 Cold case (general MLI): Eclipse . . . . .	v
D.10 Dynamic Thermal Study (general MLI) . . . . .	v
E.1 Block diagram of the major elements of CryoSat OBDH architecture [4] . . . . .	vi

# List of Tables

1.1	General instruments parameter . . . . .	4
1.2	Chirp Generator Data . . . . .	5
1.3	SSPA Generator Data . . . . .	5
1.4	Overview measurements goal . . . . .	5
1.5	Operational modes' data . . . . .	6
2.1	CryoSat velocity budget estimation. . . . .	12
2.2	$\Delta V$ budget . . . . .	13
3.1	Frequency band allocation for different satellite communications based on [5] . . . . .	21
3.2	Estrack ground station facilities [6] . . . . .	21
3.3	X-band parabolic antenna [1] . . . . .	22
3.4	Sputnix SXC-XTX-01 transmitter [7] . . . . .	22
3.5	S-band antennas [1] . . . . .	22
3.6	ISISPACE S-band transceiver [8] . . . . .	23
3.7	X-band link budget downlink . . . . .	23
3.8	X-band link budget downlink results . . . . .	23
3.9	S-band link budget downlink . . . . .	24
3.10	S-band link budget downlink results . . . . .	24
3.11	S-band link budget uplink . . . . .	24
3.12	S-band link budget downlink results . . . . .	24
3.13	Mean duration and number of contacts . . . . .	24
3.14	Data Rate and the total amount of downloaded Data . . . . .	25
3.15	Propulsion technologies comparison[9] . . . . .	26
3.16	Tank weight comparison . . . . .	29
3.17	Feed-System Module components . . . . .	30
3.18	Pointing Requirements . . . . .	31
3.19	CryoSat nominal power demand for different modes[4]. . . . .	35
3.20	CryoSat power budget breakdown . . . . .	36
3.21	Results comparison . . . . .	37
3.22	Solar array specifications [10] . . . . .	37
3.23	Results comparison . . . . .	38
3.24	Battery specifications [11] . . . . .	38
3.25	Operative Temperature Ranges . . . . .	40
3.26	Multinodal Thermal Analysis Results . . . . .	41
3.27	Nodes' external optical properties . . . . .	42
3.28	Statistical Mass Distribution Estimation . . . . .	44
B.1	Spacecraft Injection Accuracy for circular orbit of Dnepr Launcher . . . . .	ii
B.2	Maximum Launcher Acceleration . . . . .	ii
E.1	CryoSat OC performance estimation . . . . .	viii
E.2	OC results . . . . .	ix
E.3	ERC32 TSC695F(L) SPARC V7 processor specifications [12] . . . . .	ix

# 1 | Mission Overview

ESA's CryoSat mission, launched on 8 April 2010, was the third mission to operate within the framework of the Living Planet program aimed at studying different aspects of Earth's environment exploiting the advantages of space observation. The launch of the CryoSat followed by less than one year those of GOCE and SMOS, which aimed respectively at mapping Earth's gravity field and soil moisture and ocean salinity.

The history of CryoSat's mission can be traced as early as in 1998 when it was first proposed by Prof. Duncan Wingham to survey the planet's cryosphere and it would have been operative since 2005 if the first specimen had not failed to be put on orbit because of a launcher malfunctioning. This is the reason why, informally, the number 2 is dropped from the currently operating satellite name which is, and will be throughout this report, simply called CryoSat.



Fig. 1.1: CryoSat mission's logo

The mission, currently in its thirteenth year, has provided priceless information about the interaction between ice and climate and climate change by measuring the changes in the thickness and extension of the ice sheets floating in the oceans or covering landmasses in the polar regions of Earth.

## 1.1 Mission Objectives

The aim of the mission, as anticipated, is to study the Earth's cryosphere by collecting and transmitting the scientific data produced by the on-board payload. The high-level scientific objectives of the mission can be summarized as follow:

- Measure the extent of thinning of the ice sheets due to climate change.
- Determine fluctuations in the mass of the Earth's major lands and marine ice fields.
- Determine regional trends in Arctic perennial sea-ice thickness and mass.
- Determine the contribution that the Antarctic and Greenland ice-sheets are making to mean global rise in sea level.
- Observe the seasonal cycle and inter-annual variability of Arctic and Antarctic sea-ice mass and thickness.
- Observe the variation in the thickness of the Earth's ice caps and glaciers.

CryoSat completed its major mission objectives after eight years of successful operations by demonstrating technologies that opened new observing opportunities and scientific streams in other disciplines. The mission's operations were extended as a result of its success, and a new set of objectives was established:

- Assess time space variability of ice-sheet margins, glaciers and ice caps at high spatial resolution.
- Assess mesoscale and large scale oceanic variations in Polar regions in support of climate and emerging operational services.
- Assess the impact of product latency to support different operational and forecasting services.
- Extend the current data record into the next decade and improve the current geophysical retrievals and explore the option of generating new dataset from innovative methods.
- Assess the contribution to cryosphere meteorology: snow fall and melting on sea-ice and land-ice over polar regions.
- Monitor inland water, river discharge and lake volume variations at high spatial resolution.

### 1.1.1 Mission Rationale

Missions like CryoSat, aimed at checking the effects of the climate changes, are fundamental to understand the risks for the planet. The ice glaciers are made of ice ranging from several hundreds to several thousands years old; as a consequence they are capable to provide a scientific record of how climate has changed over time. For this reason, through their study, it is possible to gain valuable information about how fast the planet is warming. The glaciers melting significantly increases the amount of water in the ocean, contributing to the global sea level rise. Human activities are at the root of this phenomenon: the rise of the sea level is responsible for the increase in the coastal erosion but it has also a worldwide impact on the disruption of weather patterns: floodings and storms are becoming less predictable and more intense over the years.

The data obtained by the CryoSat mission showed that extreme ice melting events in Greenland have become more frequent and intense over the past 40 years: during the past decade Greenland has averaged 357 billion tons of ice melt per year while in 2012 it reached the maximum of 527 billions of tons. These first observations of Greenland runoff from space can also be used to verify how climate models simulate ice sheet melting which, in turn, will allow improved predictions on how much Greenland will raise the global sea level in the future as such extreme weather events become more common. These predictions can give a wide range of results, in part because of uncertainties associated with simulating complex ice-melt processes, including those associated with extreme weather. These new spaceborne estimates help to understand these complex ice-melt processes better, improve the ability to model them, and thus enable the scientific community to refine the estimates of future sea-level rise. Looking further to the future, the Copernicus Sentinel Expansion mission CRISTAL will ensure that Earth's vulnerable ice will be monitored in the coming decades. In the meantime, it is imperative that CryoSat remains in orbit for as long as possible to reduce the gap before these new Copernicus missions are operational.

## 1.2 Functional Analysis

This chapter is intended to present the functional analysis of the CryoSat mission, starting from the analysis of the declared mission objectives in Chapter 1.1 and then going into detail at system level. The functionalities will be then declined into requirements in the Appendix F.

Being an Earth observation mission most of the design was carried out with the aim of meeting the scientific aims of the mission, the details of the compromises made and the solution to answer the reported functionalities will be presented in the relative chapter devoted to the specific system.

### 1.2.1 High-level functionalities

In this section are reported the high-level functionalities derived from the mission objectives in order to highlight the main driver parameters to fulfill the objectives of the mission.

- **F.1** Reach the final orbit
- **F.2** Acquire real time attitude and position knowledge
- **F.3** Communicate with ground
- **F.4** Maintain a suitable pointing
- **F.5** Perform the scientific measurements
- **F.6** Operate continuously for all the nominal mission duration
- **F.7** Preserve the global coverage and passage scheme
- **F.8** Provide power to all the subsystems
- **F.9** Protect all the devices from the environment

- **F.10** Guarantee the respect of the operability conditions of the devices present on the platform
- **F.11** Monitor the subsystems conditions
- **F.12** Meet the computational demand of the subsystems

### 1.2.2 Payload Functionalities

In this section are reported the main functionalities that the payload on-board must perform in order to fulfill the high-level functionalities reported in the previous section.

- **F.5.1** Measure the ice thickness
- **F.5.2** Associate ice data to the position and time of acquisition
- **F.5.3** Adapt the measurement operations to the satellite position
- **F.5.4** Provide alternative measurement way in case of malfunctioning
- **F.5.5** Perform periodic calibration of the instrument

The payloads equipped in CryoSat capable to perform the declared functionalities will be broadly discussed in section 1.3.

## 1.3 Payloads

The satellite, as already mentioned, is designed for ground observation, thus it has to maintain a precise nadir pointing. The scientific payload consists of three instruments located in the ground-facing surface of the platform as they can be used simultaneously without the need for an attitude change. The three items are:

- **DORIS** or Doppler Orbitography and Radiopositioning Integration by Satellite
- **LRR** or Laser RetroReflector
- **SIRAL** or SAR (Synthetic Aperture Radar) Interferometer Radar Altimeter

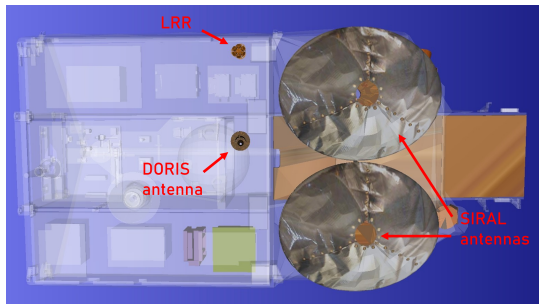


**Fig. 1.2:** Payload position [1]

Each of them is described in the next sections of this report. An important part of the measurement process, external calibrations, are usually done on transponders and flat water surfaces. Such measurements were taken throughout the commissioning phase and at regular intervals after that. They are always carried out to minimize the influence on data return, and they are occasionally carried out in combination with Collision Avoidance Manoeuvres, which are necessary to avoid space debris in collision paths. Eventual residual errors are corrected via independent and contemporaneous in situ measurements.

### 1.3.1 SIRAL

CryoSat's main payload is a radar altimeter called SIRAL, which stands for Synthetic aperture radar and Interferometric Radar ALtimeter. The altimeter is derived from the conventional pulse-limited altimeter called Poseidon-2 on board the US-French Jason-1 mission. The SIRAL concept is based on a Ku-band nadir-looking radar which can be operated in the conventional

mode over oceans. Over terrain (ice or land) the "advanced mode" uses Doppler filtering for the enhancement of the along-track resolution. A second antenna and receiving channel provides a second take of the scene which is used for surface height retrieval as it is usually done with SAR interferometry.



**Fig. 1.3:** CryoSat bottom view, artistic impression

Before going more into details, a first list of SIRAL parameters can be retrieved. Tab1.1[13] shows a set of data which are constant among any of the instrument's operational modes:

Parameter	Value
RF frequency	13.575 GHz <sup>1</sup>
PRF Timing	Regular in LRM, burst in SAR/SARIn
RF peak power	25 W
Antenna size	2 reflectors 1.2 m x 1.1 m, side-by-side
Antenna beamwidth (3 dB)	1.08° (along-track) x 1.2° (cross-track)
Antenna footprint	15 km
Antenna Gain	42 dB
Range resolution	~45 cm
Instrument mass (with antennas)	72 kg

**Table 1.1:** General instruments parameter

The system consists of three major subsystems:

**Antenna Subsystem** It consists of two Cassegrain antennas mounted side by side forming an interferometer. The antennas are identical but one is used both to transmit and receive while the second is used only when in SARIn mode. They are elliptical to answer the need to fit inside the launcher's fairing and to satisfy the beamwidth requirements. They are mounted in the nose of the satellite, close to the star trackers on a special structure with great thermoelastic stability and are thermally insulated from the environment.

**Digital Processing Unit** It is responsible for the control of the instrument and communication interfaces with the rest of the satellite. The clock frequency of 10 MHz is provided by DORIS. A digital chirp generator provides the modulated radar pulse for transmission. It operates with a sampling rate of 160 MHz, followed by an analog multiplier section expanding the pulse bandwidth by a factor of 16, up to 350 MHz. This configuration ensures the pulse-to-pulse coherence required for the SAR modes. A FFT module, performs the Fourier transformation on some echoes to generate the echo waveforms needed to drive the software tracking loops.

**Radio Frequency Unit** The Radio Frequency Unit receives the chirp signal from the digital unit and multiplies its bandwidth by a factor 16 using analogue circuitry. Signal amplification for transmission is achieved by a solid state power amplifier (SSPA), with an RF peak power output of 25 W.

Some technical data of the chirp generator and SSPA are now reported:

Parameter	Value
Frequency	4.08 GHz
Bandwidth	350 MHz
Signal duration	51 $\mu$ s
SNR	30 dB

**Table 1.2:** Chirp Generator Data

Parameter	Value
Frequency	13.575 GHz
Peak power	> 25 W
Gain	9 dB
Amplitude ripple	0.2 dB in 350 MHz
Efficiency	24 %

**Table 1.3:** SSPA Generator Data

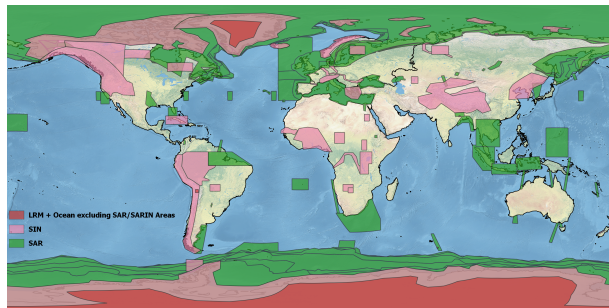
## SIRAL Operational Modes

The science requirements demand CryoSat to measure variations in ice thickness of perennial sea and land ice fields to the limit allowed by natural variability, on spatial scales varying over three orders of magnitude. The precision of the measurements are expressed in terms of cm of yearly ice equivalent thickness variations. In Tab.1.4 are reported the measurement goals for each specific parameter.

Parameter	Coverage km <sup>2</sup>	Science req.	Measurement accuracy
Arctic sea ice	$10^5$ for Lat $\leq 50^\circ$ lat	3.5 cm/yr	1.6 cm/yr
Ice sheets			
Regional scale	$10^3$ to $10^4$	8.3 cm/yr	3.3 cm/yr
Antarctica	$10^6$	0.76 cm/yr	0.17 cm/yr

**Table 1.4:** Overview measurements goal

CryoSat was designed to acquire data continuously while orbiting the planet, switching automatically between its three measurement modes according to a geographic mode mask to satisfy these requirements. In Fig.1.4 is shown the Geographical Mode Mask (v 4.0), operational from Week 34 2019 (19 August - 26 August) onwards.

**Fig. 1.4:** SIRAL Geographic Mode Mask, week 34, August 2019

The three measurement modes are:

- **LRM** (Low Resolution Mode): Similar working principle of conventional pulsedwidth-limited altimeters. It uses a single receive channel, low PRF (kept constant at about 2 kHz), and the data rate is low. Before transmission data are averaged on board, which occurs after performing the FFT (Fast Fourier Transform). This mode is used where the slopes of the surfaces are low (i.e. ice caps and oceans, where the topography is homogeneous, at least as large as the antenna footprint of 15 km).
- **SAR** (Synthetic Aperture Radar): It uses a single channel but higher PRF. The along-track horizontal resolution of the altimeter is enhanced by exploiting the Doppler properties of the echoes as they cross the antenna beamwidth. The result is equivalent to decomposing the main antenna beam into a set of 64 narrower synthetic beams in the along-track direction. The footprints of the different sub-beams over a flat surface are adjacent rectangular areas, about 250 m wide in along-track and as large as the antenna's cross-track footprint (up to 15 km).

km). Hence, a large number of independent measurements are available over a given area this enhances the accuracy of the measurement. The echoes are transmitted to ground in the time domain, without any averaging. Hence the data rate is significantly higher in this mode. To allow the decomposition into the 64 synthetic beams the instrument operates in burst mode and the PRF is about ten times higher.

- **SARIn** (SAR Interferometric): The objective is to provide improved estimates over variable topography. The combination of SAR and interferometry allows to determine the arrival direction of the echoes both in the along- and cross-track directions by comparing the phase of the two received signals. The directivity is necessary to derive the height of the surface from the range measurement of the radar. This is done by using narrow-band tracking pulses transmitted in between successive wide-band measurement bursts. Both channels are active, the data are transmitted to ground in the time domain and double the size of SAR mode. This mode is mostly used for ice sheets margins.

The details of the different operational modes are shown and compared in Tab.1.5.

Parameter	LRM	SAR	SARIn
Receive chain	1 (left)	1 (left)	2 (left and right)
Samples per echo	128	128	512
Range window	60 m	60 m	240 m
Bandwidth	350 MHz	350 MHz	350 MHz
PRF	1970 Hz	17.8 kHz	17.8 kHz
Tx pulse length	49 $\mu$ s	49 $\mu$ s	49 $\mu$ s
Burst length	N/A	3.6 ms	3.6 ms
Pulse/Burst	N/A	64	64
Burst repetition interval	N/A	11.7 ms	46.7 ms
Azimuth looks (46.7 ms)	91	240	60
Tracking pulse bandwidth	350 MHz	350 MHz	40 MHz
Size of tracking window	60 m	60 m	480 m
Averaged tracking pulses (46.7 ms)	92	32	24
Data rate	51 kbit/s	11.3 Mbit/s	2 x 11.3 Mbit/s
Power consumption	95.5 W	127.5 W	127.5 W

Table 1.5: Operational modes' data

SIRAL was selected because of the high precision required by the mission and for its main characteristics, which are:

- The capability to operate in different measurement modes, lowering resolution and power demand over areas where extreme accuracy is not required.
- Digital chirp generation with pulse to pulse coherence for Doppler processing.
- Solid State Power Amplifier (SSPA) in Ku-band with high performance (25 W).
- Dual antennas forming an interferometer, mounted on an optical bench together with star-tracker heads, ensuring the accurate knowledge and stability of the interferometric baseline orientation.
- Two receiver chains matched together with very low distortions.
- Compared with conventional altimeters, it possesses the capability to locate a resolution cell in the 3 dimensional space.

The instrument was made fully redundant as any electronic component is duplicated. For what concerns the antennas, the system is one failure tolerant as it can continue to operate even though the SARIn mode is not possible with just one antenna.

### 1.3.2 DORIS

In order to transform the data gathered by SIRAL into something scientifically meaningful the satellite must know its exact position at the time in which measurement are performed. For this reason CryoSat features a second instrument, a DORIS receiver, that allows precise orbit determination and tracking.

This system relies on a global infrastructure developed throughout the years by the CNES and IGN with the aim of continuously covering the satellites trajectory[14].

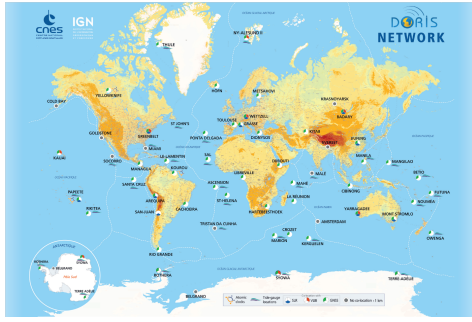


**Fig. 1.5:** DORIS ground station locations

The first is the main measuring frequency and is less affected by ionospheric errors because of its higher frequency. The latter is modulated to provide information about timing, meteorological and engineering data. Its presence is also fundamental to reject ionospheric errors and delay of the main signal.

The receiver on board measures the shift in frequency of the received signals caused by the Doppler effect to infer information about the relative velocity with respect to the GS. In the radial direction the accuracy is better than 0.5 mm/s. The orbit position accuracy is in the order of 2 ÷ 6 cm. It is worth mentioning, however, that such performances are not reached instantaneously, the orbit is calculated with increasingly precision as more data are gathered. DORIS estimates a positioning error close to 10 cm after 3 hours of data, 2.5 cm after 30 days[15]. The on board apparatus comprises three elements:

- A fixed omnidirectional quadrifilar helix antenna. It is positioned in the bottom surface and is used to receive both frequencies.
- A receiver performing the measurement of the Doppler shift of the two beacon signals.
- An Ultra Stable Oscillator producing the reference frequency with a stability of  $5 \times 10^{-13}$  over a period of 10 to 100 s.

The DORIS receiver weights 15 kg and requires 20 W of power under nominal conditions but it can reach up to 30 W during warm up. Eventually, its datarate is 4 kbit/s.

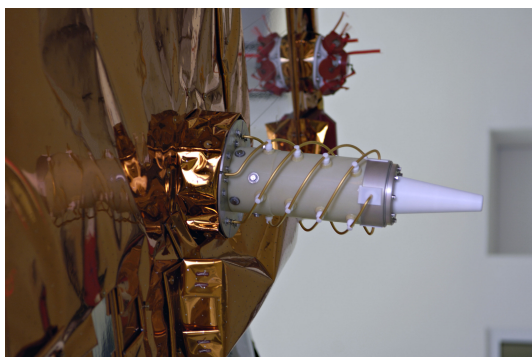


**Fig. 1.6:** DORIS antenna

Each GS is composed by a beacon, an omnidirectional antenna and a set of meteorological sensors. Of all the stations, three operate as master, they are permanent and responsible for the synchronization of the system to the IAT. Two frequencies are transmitted:

- 2036.25 MHz (S-band)
- 401.25 MHz (UHF-band)

To summarise the DORIS instrumentation provides the satellite with:

- On ground Precise Orbit Determination and Ionospheric Modelling.
- Real time orbit determination for on board attitude and orbit control.
- Precise time reference based on IAT and a precise 10 MHz reference signal.

### 1.3.3 LRR

The Laser RetroReflector is a passive optical device, positioned at the nadir surface near the DORIS antenna. It serves as additional tool and backup for precise orbit determination. As DORIS, it can operate only thanks to a ground infrastructure, in this case the international laser tracking network. The instrument has a FOV of  $\pm 57.6^\circ$  (obtained via 7 actual retroreflectors) and allows for range measurement above  $20^\circ$  elevation angles at all azimuths from the ground. For any aspect angle the predicted RMS of the error is below 6 mm. The prism is made of fused quartz, the reflective surface coating of aluminum. The laser wavelength that can be employed are between  $310 \div 1450\text{ nm}$ . The mass of the instrument is 0.36 kg[16]. From the picture below it is possible to notice that the white body of the instrument raises slightly above the edges of the optic chamber. This helps containing the contamination risk.

By reasoning on the possible reasons that lead the CryoSat engineers to opt for the installation of such device it is possible to infer several rationales:



**Fig. 1.7:** CryoSat's Laser RetroReflector

- The redundancy of the satellite tracking could have been achieved by doubling the DORIS hardware (as done with the main payload i.e. SIRAL) but this would have implied a greater cost and complexity.
- The laser retroreflector is passive, thus it is intrinsically characterized by a greater reliability.
- The LRR can operate even in case of an emergency, provided that the ADCS is capable of maintain the bottom surface of the satellite nadir pointed so that the GS has the possibility to track it.

## 2 | Mission Analysis

The aim of this chapter is to first present the result of the investigation made by considering the mission as a whole. After that it will be carried out an in-depth study on orbital analysis and mission phases in which the CryoSat mission can be divided into.

### 2.1 Orbit

Cryosat was injected directly into its final orbit, through the Ukrainian-Russian launcher Dnepr (see appendix B). Now discontinued, it was a three stage liquid engine LEO launcher. A copy of the user manual issued in 2011 is available at this link. This launcher was selected instead of the originally intended Russian Rockot after the failure of the same during the launch of CryoSat1.

The orbit selected for CryoSat is the result of several trade-offs. Indeed the altitude is a compromise between the radar link-budget, the launcher capabilities and the air drag, while the inclination was selected as a compromise between coverage of very high latitude regions and the density of cross-overs. The nominal Keplerian elements of the orbit and its main characteristics[4] are:

• $a = 7095.348557673 \text{ km}$	<b>Type</b>	Near circular, polar, low earth orbit
• $e = 0.001406846$	<b>Mean altitude</b>	720 km
• $i = 92.000678420^\circ$	<b>Repeat period</b>	5344 revolutions (with 30 days sub-cycle)
• $\Omega = 129.997076727^\circ$	<b>Orbit control</b>	$\pm 5\text{km}$
• $\omega = 115.619512345^\circ$		

From the nominal Keplerian elements one can easily deduce that the orbit is polar but not a Sun-Synchronous Orbit (SSO). Indeed, under the assumption that only J2 effect is acting on the orbit, according to the formula:

$$\frac{d\Omega}{dt} = -\frac{3}{2}J_2 \left( \frac{R_{\text{earth}}}{a} \right)^2 \frac{1}{(1-e^2)^2} \sqrt{\frac{\mu_{\text{earth}}}{a^3}} \cos(i) \quad (2.1)$$

the RAAN rate is equal to  $0.239^\circ/\text{day}$  (positive eastward). As it does not match the rate at which the Sun moves (equal to  $0.986^\circ/\text{day}$ ) the local solar time on each passage is not constant. In order to have a SSO with the given semimajor axis the inclination would have had to be equal to  $98.28^\circ$ . The fact that the orbit is not a SSO implies, as the lighting conditions are not constant, that there would be some orbits in which the satellite flies on the dawn-dusk line hence with one side always opposite to the sun. In addition, not having selected a sun-synchronous orbit clearly makes more complicated to design the thermal control system and the position of the star sensors as the relative direction of the sunlight is not fixed during the orbit.

In order to understand the trade off made when selecting the operational orbit, the nominal one has been compared with a SSO characterised by the same semimajor axis. Such analysis was carried out with the aid of GMAT[17]. The first aspect that was considered is the eclipse duration (it is a conservative estimation as umbra and penumbra were considered altogether). By comparing the two upcoming figures it is easy to deduce that a SSO would have been better from the power availability point of view, since the maximum eclipse duration is lower and the time spent without eclipse at all is longer.

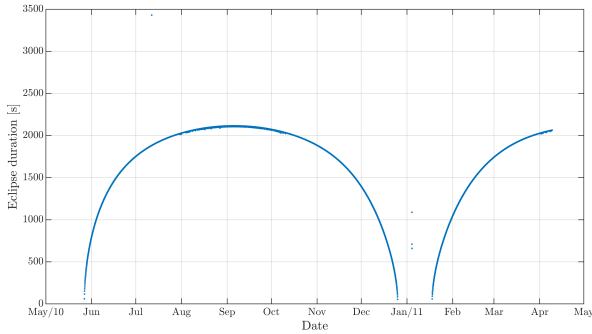


**Fig. 2.1:** Duration of the eclipses in the first year following the launch date April 9<sup>th</sup> 2010

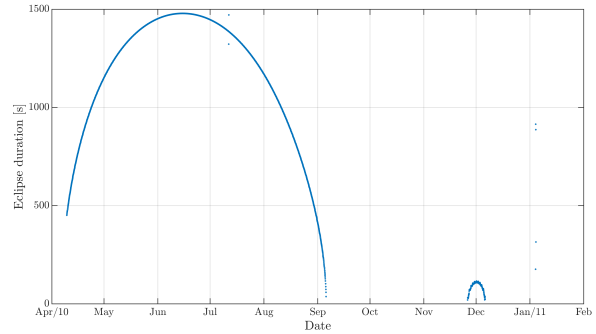


**Fig. 2.2:** Duration of the eclipses for SSO for the year starting on April 9<sup>th</sup> 2010

The second point to be considered was the visibility with the selected ground station: the ESA facility at Salmijärvi, near Kiruna. A mask angle of 5° was considered. The analysis was performed for 30 days i.e. the duration of the subcycle of the nominal orbit.

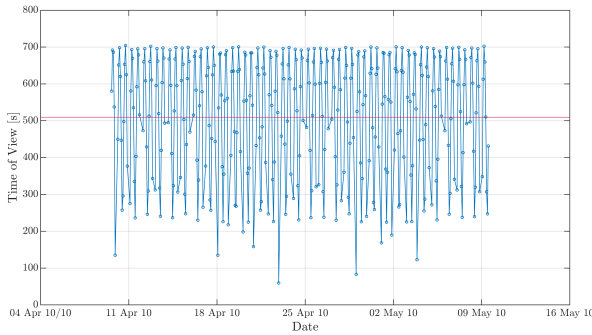


**Fig. 2.3:** Time of visibility from Kiruna of the nominal orbit

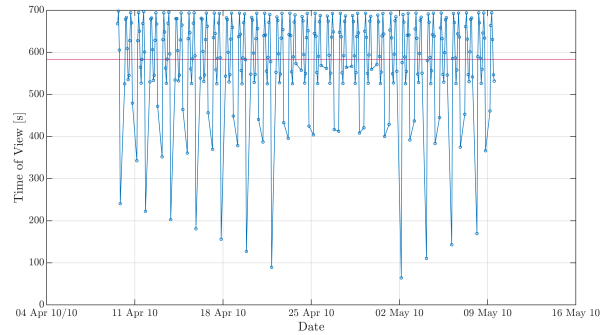


**Fig. 2.4:** Time of visibility from Kiruna of the SSO

The last two figures reveal once again that the SSO would have been more advantageous as the average visibility time for the SSO (red line in the plots) is higher. Considering CryoSat's nominal orbit, on average, of all the 14 complete orbits completed per day, 3 are blind (i.e. no radio contact is possible). Data collected during these times shall be stored and the link budget shall be designed considering that at each passage the satellite must download the data relative to the actual orbit plus part of those collected during blind orbits.

The last feature to be considered was the Earth's surface coverage. For the same amount of time of the last analysis the two ground tracks were compared to establish which one covers better the polar region.

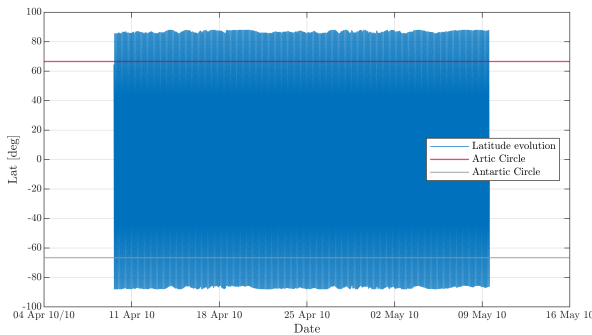


**Fig. 2.5:** Latitude vs time on nominal orbit

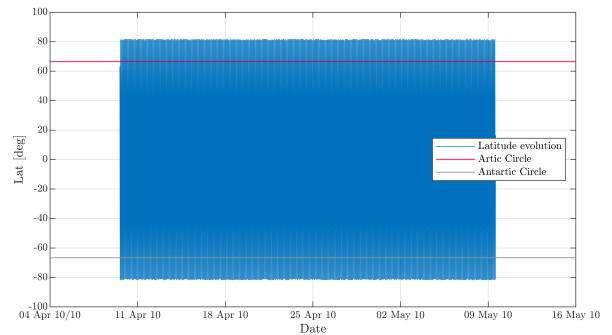


**Fig. 2.6:** Latitude vs time on SSO

This plots allow to appreciate how the selection made allowed to better cover the polar regions as the satellite could reach higher latitudes than in a SSO. The chosen orbit allows to reach  $88.1^\circ$  of latitude, while the SSO is limited to  $81.8^\circ$ . Moreover the time spent by the satellite above the polar circles on the nominal orbit was found to be (for the considered month) equal to 7.7754 days, while it is equal to 7.3218 days in the second case. Since Cryosat is a scientific mission, it has been preferred to improve coverage and density of passages at high latitudes rather than features like visibility time and eclipse duration.

One additional important aspect of the orbit, regardless of the sun-synchrony, is the fact that it is retrograde. The main payload of CryoSat, SIRAL, operates via SAR technique. According to this scanning technique, the aperture of the antenna is increased by the distance travelled by the device in the time the radar pulses gets back to the source with positive effect on the instrument resolution. In a retrograde orbit, the satellite moves faster with respect to the surface enhancing this effect.

### 2.1.1 Orbit Evolution

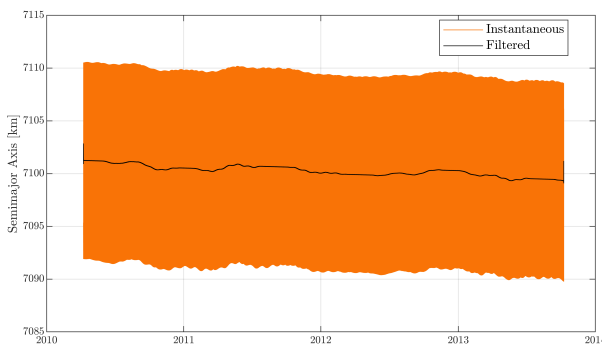
To meet the science goals, as mentioned, a control band of 10 km width was imposed on the orbit (i.e. the orbit control shall maintain the spacecraft within such band centered on the nominal orbit).

Given the orbital region, the expected sources of disturbances are, presented in decreasing order:

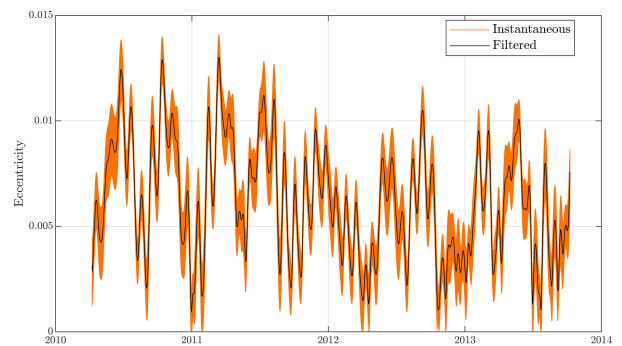
- Earth's gravitational field harmonics  $2 < n < 5$
- Lunar gravity
- Sun gravity
- Solar radiation pressure (SRP)
- Drag

The last one may be higher than the SRP depending on the solar activity as it affects the density of the atmosphere.

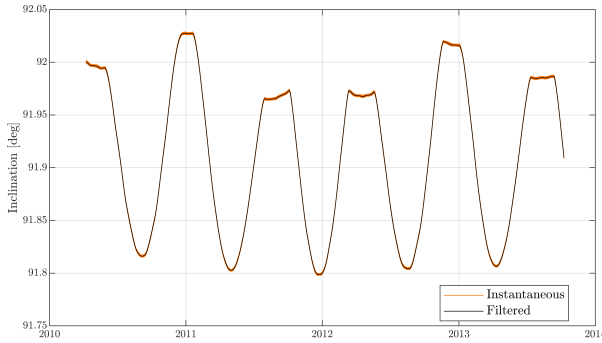
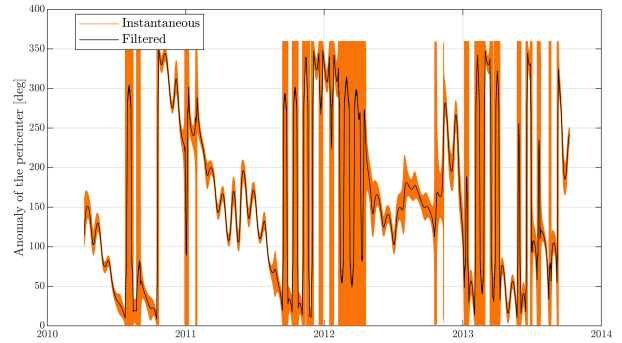
In the next plots are reported the results of the study of the degeneration of CryoSat's orbit. All the aforementioned disturbances were considered (some simplification were applied such as constant attitude and uniform atmospheric data valid for average sun's activity). In the plots the black line represents the results averaged on the single day (24 hours) as the Keplerian elements showed appreciable variations also within the orbital period. The RAAN evolution is not plotted as it varies almost linearly with time.



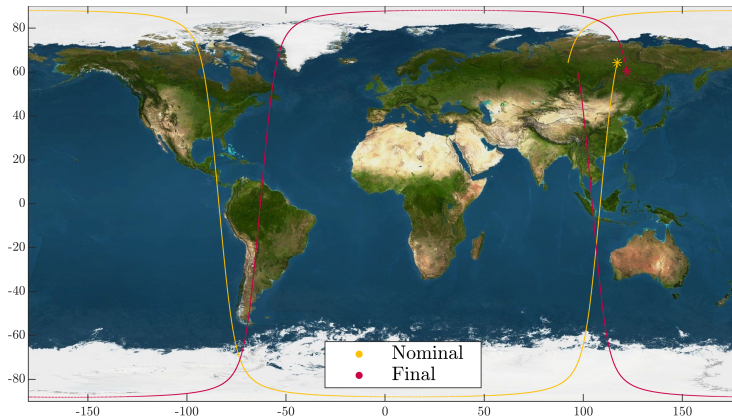
**Fig. 2.7:** Semimajor axis evolution



**Fig. 2.8:** Eccentricity evolution

**Fig. 2.9:** Inclination evolution**Fig. 2.10:** Anomaly of the Pericentre evolution

It was said that the orbital motion would repeat itself after 369 days (circa), or 5344 orbits. If no correction is applied during three of these cycles the following situation can be observed:

**Fig. 2.11:** First ground track vs ground track after 3 full (nominal) cycles with no corrections

The previous figure allows to appreciate the shift between the two after roughly 3 years. Hence, it is possible to conclude that performing periodical orbital maintenance is necessary to achieve the mission goals which are highly dependant on the ground pattern.

### 2.1.2 Orbital Maintenance and $\Delta V$ Budget

As the previous chapter showed, all the Keplerian elements are subjected to changes, some like the RAAN almost linearly, others in a more erratic way. These changes, despite being small in terms of absolute value, cause large variations in the ground tracks as Fig. 2.11 reported. The orbit maintenance is performed by means of the reaction system. Considering its nominal performances the following rough estimation of the costs in term of  $\Delta V$  can be obtained:

Correction	Frequency	Cost [m/s]	Total Cost [m/s]
Insertion	1/Lifetime	4.632	9.246
Shape	1/Month	0.018	1.506
Inclination	3/Year	0.723	16.257
Collision Avoidance	2/Year	0.318	2.226
<b>Total</b>			<b>29.235</b>

**Table 2.1:** CryoSat velocity budget estimation.

The total costs refer to the nominal life duration of 3.5 years. A margin of 100% on the result was applied to the computed costs for insertion errors compensation, shape and inclination corrections. This margin is justified by the simplifying assumptions made: no disturbances while thrusting and inclination corrected with instantaneous manoeuvres. For the insertion the maximum errors on

inclination and semi-major axis, taken from the launcher's manual have been considered. Collision avoidance manoeuvres did not consider any margin, as they represent the arbitrary reduction of 500 m of the perigee height. The shape adjustment were assumed to occur once per month, this is not true as they are deeply influenced by the Sun's activity hence the drag is not constant. The irregularity of such intervention is proved by Fig. 2.12. The inclination adjustments have been considered to be performed to correct the long period variation in such parameter i.e. to maintain the peaks of the sinusoid in Fig. 2.9 at constant height.

The  $\Delta V$  here computed translates into a propellant mass fraction of 4.05%, i.e. for the total initial mass of 724.6 kg (as declared) the propellant mass should be 29.35 kg (without margin on the mass). This value, however, is not likely to represent the complete propellant mass on board, as it did not include the propellant for attitude control. Therefore, for the analysis of the reaction system architecture the true mass of propellant has been considered. The detailed  $\Delta V$  budget for the 3.5 year mission considered by the designer of the mission is reported in the upcoming table[4]. The table also reports the values for the initially expected life extension to 5.5 years, such extension was forecast at the expense of the margin on the propellant which were dropped from 12% to 1%.

Phase	$\Delta V$ (m/s)	Propellant Mass (kg)
<b>Orbit control</b>		
Orbit Acquisition	8.28	
Orbit Maintenance	1.8 <sup>1</sup>	
Space Debris Collision Avoidance	1.48	
Orbit Changes	12.13	
Attitude Control During Orbit Control	0.33 <sup>2</sup>	
<i>Subtotal</i>	24.03	24.94
<b>Attitude Control</b>		
Attitude Slews for Re-orientation		0.24
Initial Rate Damping and Attitude Acquisition		0.09
Coarse Pointing (Safe Mode)		1.36 <sup>4</sup>
Fine Pointing		3.43 <sup>5</sup>
<i>Subtotal</i>		5.12
<b>Leakage and Residual</b>		
Overall External Leakage		1.00 <sup>6</sup>
Residual EOL Propellant Mass		1.62
EOL Non-Usable Propellant		0.20
<i>Subtotal</i>		2.81
<b>Total Mass</b>		32.87 <sup>5</sup>

<sup>1</sup> 2.83 due to solar cycle, <sup>2</sup> 0.35, <sup>3</sup> 2.04, <sup>4</sup> 5.39, <sup>5</sup> 36.7, <sup>6</sup> 1.57

**Table 2.2:**  $\Delta V$  budget

The real table confirms the order of magnitude of the  $\Delta V$  computed in table 2.1. It is safe to assume that the costs for the inclination correction are considered in the entry "orbit changes". The collision avoidance was overestimated, probably due to the fact that the real manoeuvre does not require to modify the orbit to the assumed extent. By analysing the table above it is safe to consider that the propellant was allocated not to answer the need to perform any deterministically designed orbital transfer, rather to perform small orbital corrections. In particular, a stochastic analysis on the cost for the injection errors compensation (starting from the declared insertion accuracy in the launcher's manual) and orbit maintenance and adjustment (based on environmental models) are clear to have been performed.

In order to meet the science goals of the mission a relaxed orbit control dead-band of  $\pm 5$ km was defined. However the actual orbital manoeuvres are scheduled to preserve the ground track scheme which is quantified by a  $\pm 1$  km error on the ground track when in the polar region [4]. Therefore

they are not performed uniformly during the year, but follow (mostly) the Sun's activity. From the web page relative to CryoSat on DORIS website the complete list and dates of manoeuvres can be retrieved.

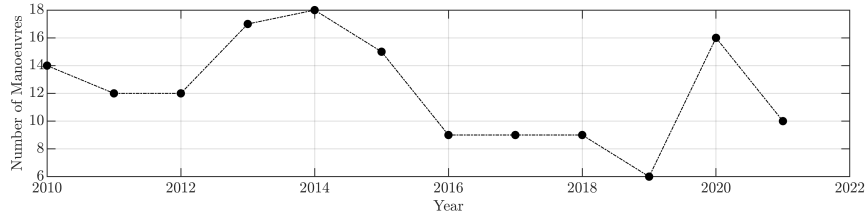


Fig. 2.12: Number of Maneuvers per Year

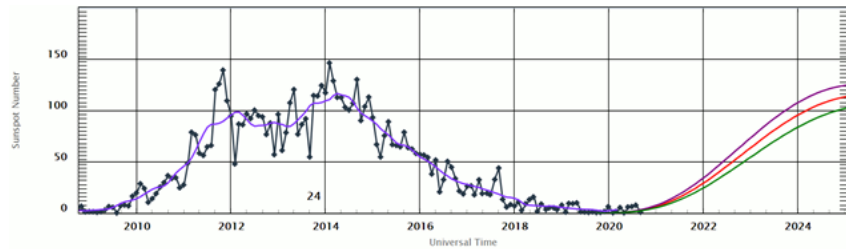


Fig. 2.13: Number of Sunspot

By comparing the two plot some conclusions can be drawn:

- The local peak in 2010 is mostly due to the manoeuvres for orbital acquisition as most of them were performed within the first month in orbit, as it correspond to a low solar activity epoch.
- The peak centered in 2014 correspond to the peak in the Sunspots number. This is logical as higher solar activity causes the disturbances (in particular drag) to increase. Then, as the solar activity diminishes, the number of manoeuvres decreases as well.
- The increase in 2020, epoch of low solar activity, can be explained instead by the fact that CryoSat was manoeuvred to phase itself with NASA ICESat-2.

Lastly, given the limited amount of propellant on board, it is safe to assume that the extension of the life of the satellite to the day of this writing was made possible by not having needed in full the amount of propellant that the designers allocated for the orbit injection error.

### 2.1.3 Orbital Decay

In this section the issue of orbit decay and deorbiting are addressed. From Fig. 2.14, considering the nominal data of the satellite it is possible to infer that the expected decay time of CryoSat would be higher than 200 years, estimation confirmed by ESA[18]. Despite such approach is highly approximated (solar cycles are neglected) it allows to catch the order of magnitude of the decay time, clearly superior than what current ESA's guidelines impose for LEO missions (i.e. 25 years). To the writers' knowledge, CryoSat is not supposed to reentry in a uncontrolled manner to meet such requirement and it is therefore likely to contribute to space pollution for two centuries at least, indeed, Fig. 2.7 showed a very little orbit size reduction. The possibility to put the satellite on a graveyard orbit outside the protected LEO region at an altitude higher than 2000 km (the second option suggested for disposal by ISO 16164:2015) was deemed even less feasible given the costs associated to such transfer. This conclusion was drawn from simple energetic analysis. The transfer to a circular orbit with an altitude of 2000 km would require 940 kg of propellant, while a transfer to a 600 km orbit (for which 2.14 predicts a 25 years lifetime) would take 65 kg of additional propellant. This is clearly a more manageable value but still almost twice the overall mass budget of propellant considered by the designers for the entire mission.

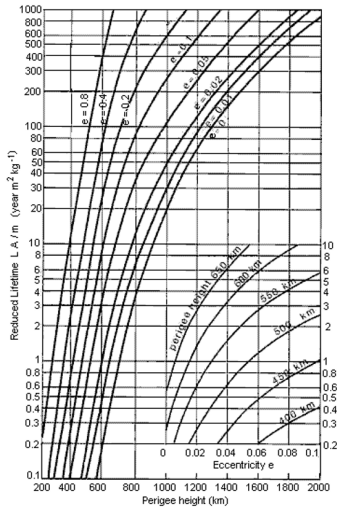


**Fig. 2.14:** Orbital decay reduced time vs perigee height and eccentricity[2]

The propulsion system has been sized just for orbit adjustment and attitude control. Thus it is not capable to perform impulsive manoeuvre that would reduce the perigee height to a point for which the decay would meet the guidelines. Additionally the satellite doesn't carry sufficient propellant for a spiral descent. CryoSat employs a cold gas thruster system with 37.6 kg of propellant. Being now the mission in its thirteenth year of life and having also performed (as part of the extended mission objective) a non originally designed manoeuvre in 2020 to be periodically phased with NASA's ICESat-2 it is highly unlikely that any deorbiting will ever be performed. CryoSat shall therefore have to be carefully tracked for the next centuries, well past its switching off, to prevent collision with other satellites orbiting in the same region.

## 2.2 Environmental Analysis

In this section the results of a brief environmental analysis are presented. The following aspects are discussed: Micrometeors and Debris, Earth's magnetic field, Atomic Oxygen and Radiations, which are all presences the designers of CryoSat had to take into account during the design.

### 2.2.1 Debris and Micrometeors

The presence of man-made debris on orbit has dramatically increased in the last decades. They represent a non negligible danger for any mission, especially those designed to operate in a LEO environment. As already mentioned CryoSat is a quite old satellite which has been operating since 2010, during this years the space panorama has changed considerably. It is interesting to notice that as of the year 2018[19] the satellite had performed thirteen collision avoidance manoeuvres using the same system it uses for attitude control (i.e. cold gas thrusters). This was made possible by better understanding and tracking of the debris left on orbit and made necessary by a net increment in the number of these objects. The current situation is well represented by the following two plots:

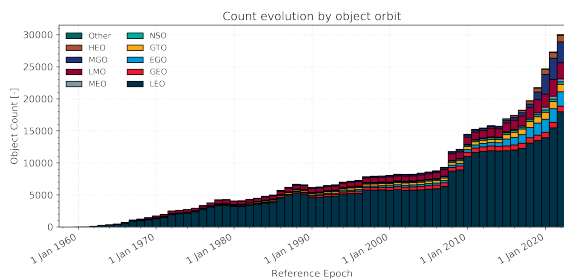


**Fig. 2.15:** Numbers of acknowledged man made object in space according to ESA[3]

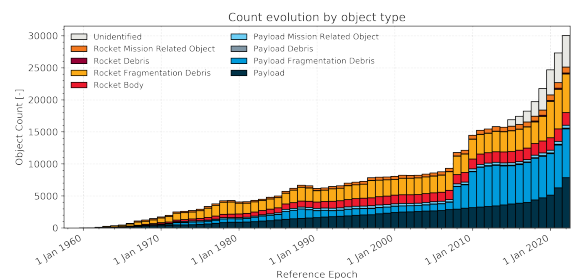


**Fig. 2.16:** Number of debris per type[3]

The next picture, obtained via MASTER (Meteoroid and Space Debris Terrestrial Environment Reference)[20] tool, allows to visualize the current situation of CryoSat's orbit, obtained averaging the mass fluxes of the thirteen years of the mission. The plot considers both micrometeors and

space debris.

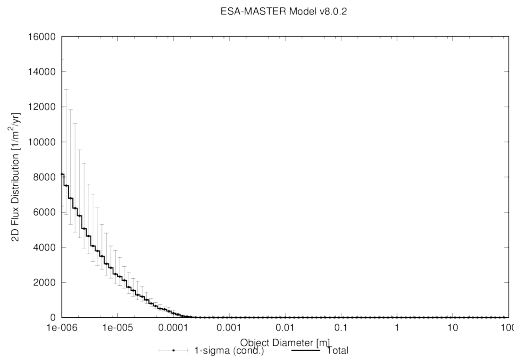


**Fig. 2.17:** Mass flux of debris and micrometeors on CryoSat's orbit

## 2.2.2 Magnetic Field

Another important aspect to consider is the magnetic field to which the satellite is exposed. Indeed, the presence of an external magnetic field represents both a disturbance for the attitude control and a resource, as it allows to employ magnetotorquers for the attitude control. These devices are actually implemented in CryoSat. This choice is clearly advantageous as it remove the need for a propellant or moving part inside the satellite. The second aspect is related to the fact that a lower magnetic field means that the ionized particles coming from the Sun (mostly) get closer to the Earth's surface, hence the satellite would be invested by a greater flux of them. The electronic components are the most affected and need to be qualified for space use. From 2.19 it is possible to notice the so called South Atlantic Anomaly i.e. a region where the magnetic field is particularly weak.

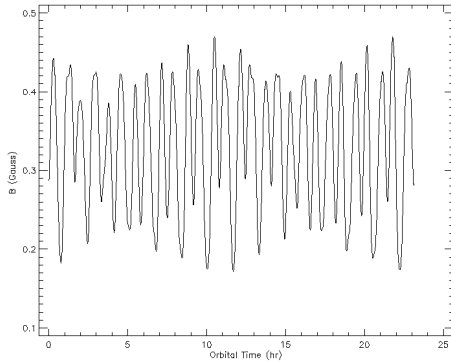


**Fig. 2.18:** Intensity of Earth's magnetic field experienced over (approximately) 24 hours of orbit

As expected the mass flux is considerably higher for smaller particles. The reduced size of the particles most likely to impact the spacecraft, however, does not ensure the complete absence of damages as their velocity is typically in the order of  $1 \div 10 \text{ km/s}$ , well sufficient to damage and puncture many of the material commonly present on a satellite.

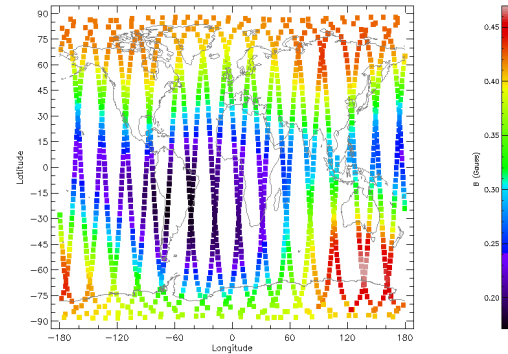


**Fig. 2.19:** Intensity of Earth's magnetic field vs satellite's location

To retrieve the previous two plots the SPENVIS[21] tool has been employed, the results include the Earth's native magnetic field only.

## 2.2.3 Atomic Oxygen

Due to its high reactivity the abundance of atomic oxygen must be investigated before the selection of the materials can be performed. Indeed the resistance to the degradation it causes is one of the main element of the trade-off for the selection of the coating, together with its optical properties. The next plot shows the amount of AO in terms of flux that, for average condition, invests the satellite during its orbit (for the retrieval of these data once again SPENVIS tool was used).

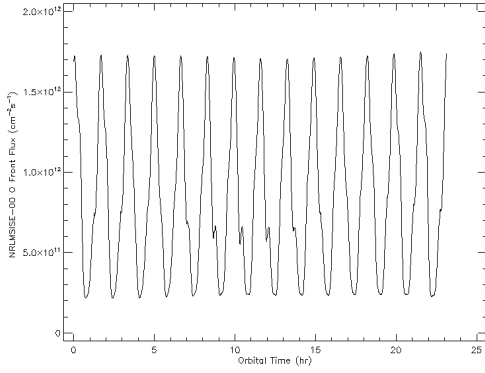


**Fig. 2.20:** Atomic Oxygen flux

## 2.2.4 Radiations

In this last paragraph a brief discussion of the effects and amount of radiation is presented, given their wide range of effect on most of the components and material of the spacecraft. Three main sources can be identified:

- Solar spectrum radiation (such as UV)
- High energy radiations ( $X/\gamma$ , rays)
- Charged particle radiations

The first mostly affects polymers which after a prolonged exposure show: loss of toughness and/or deformability, films breakage and darkening due to the formation of chromophore compounds. FEPs are in this case more sensitive than polyimides such as Kapton. The second, whose origin is either the Sun or far cosmic phenomena, cause material degradation depending on the dose. The effect mitigation against these two consists of wise material selections (use metallic materials when possible) or design composite with protective films ( $TiO_2, Ta_2O_3, Al, SiO$ ). The mitigation strategy to protect the electronic components requires to use metallic shielding (the use of material as  $Al, Ta, W$  is advisable against electrons). Despite such way is feasible, in principle, the potential loss of functionality shall be considered and redundant systems must be included. The SIRAL payload has indeed a complete redundancy of the electronics, which are also physically segregated. This allows to conclude that guaranteeing the operations of such payload was indeed a priority (as already mention whether or not it could work defined the success of the mission). While the redundancy allows to limit the effect of phenomena such as prompt effects, the physical segregation allows to reduce the chance that a particle or micrometeor puncture takes out the complete system. Concerning the satellite tracking, on the other hand, a passive system was put as backup for the DORIS receiver, rendering the backup solution insensitive to external radiation.

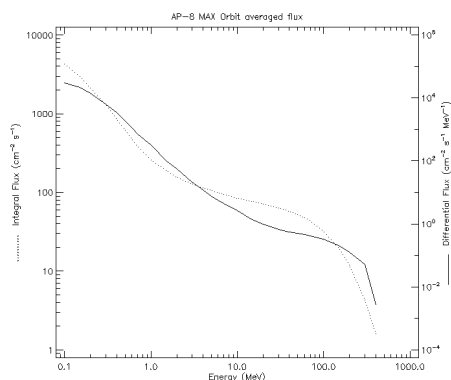


**Fig. 2.21:** Protons trapped flux

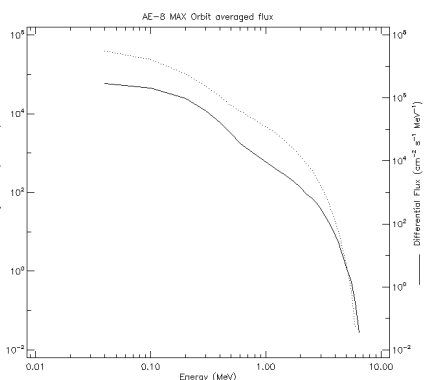


**Fig. 2.22:** Electrons trapped flux

AO is responsible for serious damages to a plethora of different materials, especially polymeric, which shows amongst the other symptoms of degradation: embrittlement, surface cracks and formation of volatile products (contamination issues). Metallic materials are (apart some exceptions such as silver) highly resistant to AO. Concerning polymeric material, by analysing the different erosion rate, the use of FEP ( Fluorinated ethylene propylene) is advisable.

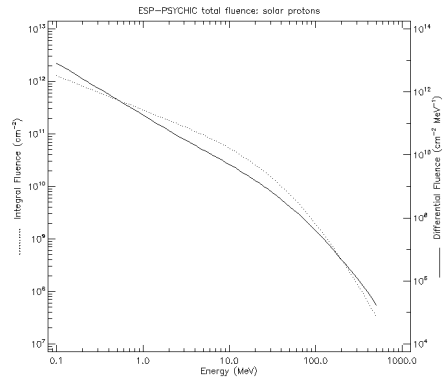


**Fig. 2.23:** Fluence of trapped particles for the thirteen years of orbit

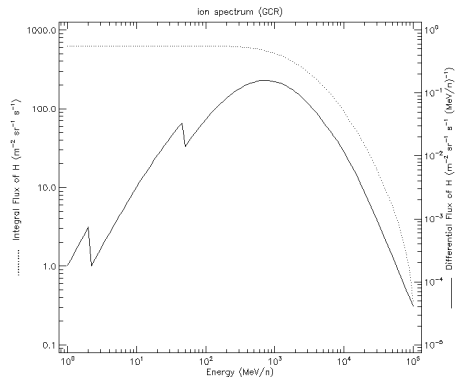


**Fig. 2.24:** Protons trapped flux of cosmic origin

The previous plots have been retrieved thanks to SPENVIS tool suite.

## 2.3 Mission Phases

### 2.3.1 Launch and Early Orbit Phase

The first phase of the mission is the so called Launch and Early Orbit phase (LEOP). It started before the launch itself, with the switch-over from ground supplied power to the satellite internal batteries. It included the launch, separation, attitude acquisition and initial switch on; in total it took three days. The launch took place at 15:57 on 8 April 2010 with the Dnepr launch vehicle (see Appendix B) from Kazakhstan. The satellite was launched into an orbital plane with an LST equal to h. 18:00 to maximise the available power during LEOP. As it came into visibility, made possible by a beacon signal emitted from the satellite to the ground station, the separation from the upper stage was performed.

The exact sequence of operations is based on the periods of visibility with the supporting ground station. The attitude system, turned on, converged towards the fine pointing mode (see section 3.3.5) and in order to achieve this the star trackers and DORIS systems had to be turned on. At the end of the LEOP all the systems but the main payload were operative. The manoeuvres required to correct the error injection were performed in the following days. They were asynchronous with respect to the other scheduled activities and were subordinated to the precise acquisition of the actual orbit.

### 2.3.2 Commissioning Phase

The next phase was the Commissioning phase, which ended with the Commissioning Review which establishes the readiness of the system to operate. It lasted about six months and can be subdivided into five sub-phases. They are partially superimposed according to link and dependencies between their activities.

- **Platform Verification:** Functional and performance verification of the satellite services (such as power, on-board data storage and downlink, and pointing) are performed.
- **Payload Verification:** In-orbit measurement of CryoSat system as a whole. The objective is to verify that everything is working correctly, to determine its performance and to make all required adjustments and tunings to the operating parameters.
- **Payload Data Segment (PDS) Verification:** It encompasses the activities required for functional and performance verification of the PDS (including payload planning, data processing, archiving, distribution and monitoring) in terms of functionality, throughput, data distribution etc. At the end of this sub-phase the data products themselves are in a condition where they may be verified scientifically.

- **Product Calibration:** The objective is to test the contents of the data products for correctness. This sub-phase is largely concerned with products at Level 1b, and the activities will generally lead to adjustment of parameters (or even some algorithms) used in the processors. This process is known as calibration.
- **Product Validation:** Here the objective is to ensure the correctness, and identify the confidence limit, of the Level 2 products. These products contain parameters expressed in geophysically meaningful units, such as surface elevation. Determining the errors in these parameters, and eventually adjusting the Level 2 data processors, requires quite extensive independent data collection. In some cases the nature of the measurements also put constraints on when the data may be acquired. As a result this sub-phase may extend well beyond the Commissioning Phase and into the operational phase of the mission.

### 2.3.3 Science Phase

The Commissioning Result review was held in November 2010 and allowed the mission to transit into the *Science Phase*, which occupies the majority of the mission. During this phase the satellite, payload and ground segment operate nominally in order to achieve the objective of the mission.

### 2.3.4 Disposal Phase

At the end of the mission lifetime the satellite will enter the *Disposal Phase*. This phase is marked by two main aspects: the *orbital decay* and the *passivation* of the system. As anticipated in section 2.1.3 regarding the *orbital decay* a strategy has not yet been decided. Regarding the *passivation*, since the main power sources of the satellite are the solar panels and Li-ion batteries, it will be necessary to ensure the complete discharge of the batteries, turn off all the electronics and, regarding the propulsion system, the tanks will have to be emptied.

### 2.3.5 Operational Modes

It is also worth mentioning the *Safe mode*, given its consequences on the whole platform. Indeed, in the event of a major on-board emergency the payload will be switched off and the satellite will automatically enter in Safe Mode, in which it can survive for a long period. It will be described from the ADCS point of view in section 3.3.5.

### 2.3.6 Conceptual Operations - ConOps

In this section, the Conceptual Operations of the mission, from the pre-launch phase to the disposal, are shown in Fig.2.25.

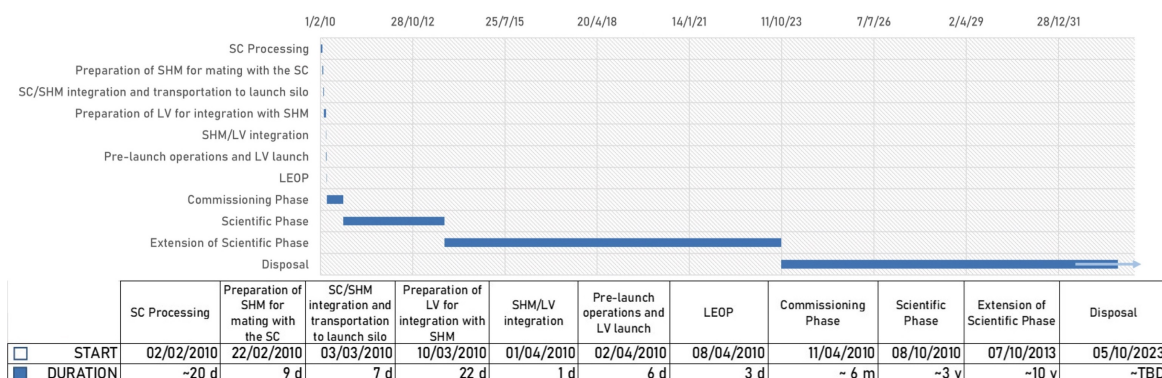


Fig. 2.25: Conceptual Operations of the CryoSat Mission

# 3 | System Analysis

In this chapter the studies on each system in which CryoSat can be decomposed are presented.

## 3.1 Telecommunication System

The TeleMetry Tracking and TeleCommand subsystem (TTMTC) is the subsystem in charge to establish a space link between the spacecraft and its associated ground stations, in the case of CryoSat the Kiruna Ground Station. Every space system requires extensive contact with the Ground Segment for control, command, communication and transmission of scientific data, health status of the spacecraft and its orbit determination. The basic data flow over a space link is made of Telemetry (TM) and Telecommand (TC) data. Thus, the TM downlink and TC uplink provide a communication channel between the spacecraft and the ground operators.

On the uplink, the On Board Data Handling subsystem (OBDH, see Appendix E) receives and decodes all commands and data for both platform and payload operations from the communications system. These commands are then directed to the appropriate subsystem or executed directly at platform level. The Telecommand can be split into:

- Direct commands to the spacecraft for reconfiguration
- Application of specific commands

While the Telemetry can be split into:

- Orbit data
- Spacecraft housekeeping data
- Payload data (science data)
- Telecommand reception status
- Memory dump data

### 3.1.1 Functionalities

According to the mission requirements the functionalities relative to the TTMTC are the following:

- **F.3.1** Comply with ESA telecommunication standard
- **F.3.2** Interface with ESA ground stations
- **F.3.3** Emit beacon signal for first acquisition
- **F.3.4** Communicate telemetry to the ground station
- **F.3.5** Receive commands from the ground
- **F.3.6** Download the scientific data to the ground station

Those functionalities has been declined into requirements in the appendix F.

### 3.1.2 Space links and frequency selection

Given the functionalities reported in 3.1.1, the s/c shall be capable to establish two different links with the ground segment for the communication of the telemetry and scientific data. The carrier frequencies selected that characterize those links are respectively the S-band (2.110 GHz in uplink and 2.200 GHz in downlink) and the X-band (8.100 GHz in downlink) accordingly with the ITU regulations [5] reported in Table 3.1. The chosen ground segment is the ESA's tracking station

network (Estrack) which is a global system of ground stations providing links between satellites in orbit and ESOC, the European Space Operations Centre, Darmstadt, Germany [6]. The core Estrack network comprises facilities located in seven different countries (see Table 3.2).

For the ground stations selection only the facilities that operate for Earth-orbit mission are considered, in particular, the stations of Kiruna (Sweden) is chosen because it can operate in the selected frequency band and it offers wide visibility windows (see 2.3 and 2.4).

RF bands	Frequency band	Utilization
S-band	2.025-2.110 GHz	Uplink
	2.110-2.120 GHz	Deep-Space Uplink
	2.200-2.290 GHz	Downlink
	2.290-2.300 GHz	Deep-Space Downlink
X-band	7.145-7.190 GHz	Deep-Space Uplink
	7.190-7.250 GHz	Uplink
	8.025-8.450 GHz	Downlink
	8.450-8.500 GHz	Deep-Space Downlink
Ku-band	14.40-14.47 GHz	Downlink
	16.60-17.10 GHz	Uplink
Ka-band	31.80-32.30 GHz	Deep-Space Downlink
	34.20-34.70 GHz	Deep-Space Uplink
	37.00-38.00 GHz	Downlink
V-band	40.00-40.50 GHz	Uplink
	54.25-58.2 GHz	Inter-satellite
	59.00-71.00 GHz	Inter-satellite
	116.0-123.0 GHz	Inter-satellite
mm-band	130.0-134.0 GHz	Inter-satellite
	167.0-182.0 GHz	Inter-satellite
	185.0-190.0 GHz	Inter-satellite
THF	191.8-200.0 GHz	Inter-satellite
	275.0-3000 GHz	Not allocated

**Table 3.1:** Frequency band allocation for different satellite communications based on [5]

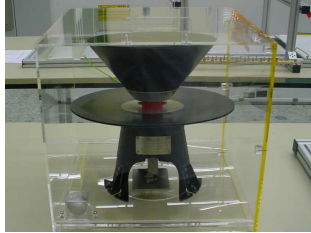
Station	Longitude	Latitude	$D_{ant}[m]$	Band
Kiruna	20° 57' 51.6" E	67° 51' 25.7" N	13/15	S/X
Kourou	52° 48' 16.8" W	05° 15' 05.2" N	15	S/X
Redu	05° 08' 43.2" E	50° 00' 01.6" N	15/13.5	S/Ka
Santa Maria	25° 08' 08.6" W	36° 59' 50.1" N	5.5	S
Villafranca	03° 57' 05.7" W	40° 26' 33.2" N	15	S/X/Ka
New Norcia (DSA1)	116° 11' 29.4" E	31° 02' 53.6" S	35	S/X/Ka
Cebreros (DSA2)	04° 22' 03.2" W	40° 27' 09.7" N	35	X/Ka
Malargüe (DSA3)	69° 23' 53.5" W	35° 46' 33.6" S	35	X/Ka

**Table 3.2:** Estrack ground station facilities [6]

### 3.1.3 Architecture

#### X-band Architecture

The X-band architecture refers to the transmitter and antenna equipped by CryoSat in order to download the scientific data produced by the payload. This architecture, reported in figure 3.1a and 3.1b, is composed of an X-band parabolic antenna [1], placed in the nadir direction of the spacecraft and 2x (for redundancy) X-band transmitters which are assumed to be [7].



(a) X-band parabolic antenna [1]



(b) Sputnix SXC-XTX-01 transmitter [7]

The equipment specifications are reported below in Table 3.3 and Table 3.4.

Gain	25.52 dB
Beamwidth	8.062°
Diameter	0.3 m

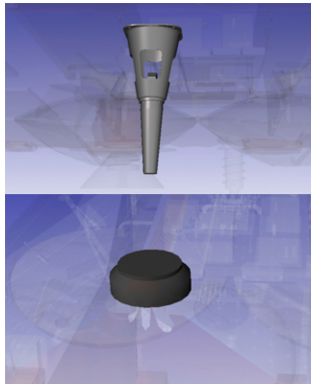
**Table 3.3:** X-band parabolic antenna [1]

Center frequency	X-band
Modulation Format	BPSK
Operating temperature	-10°C to 50°C
Size	0.089x0.093x0.027 m
Weight	0.195 Kg
Power consumption	15 W
Output power	1 W

**Table 3.4:** Sputnix SXC-XTX-01 transmitter [7]

### S-band Architecture

The S-band architecture is used to download the telemetry of the spacecraft and to upload the commands from the Ground Segment, it is composed of two antennas [1], placed in opposite faces of the satellite to guarantee the communication even in safe mode or when the pointing is not assured (i.e. during detumbling from the launcher), and 2x transceivers (for redundancy, assumed [8]) capable to operate both in transmission and receiving mode. The architecture is reported in figure 3.2a and 3.2b.



(a) S-band antennas [1]



(b) ISISPACE S-band transceiver [8]

The equipment specifications are reported below in Table 3.5 and Table 3.6.

Gain	4.306 dB
Beamwidth	98.182°
Diameter	0.1 m

**Table 3.5:** S-band antennas [1]

Center frequency	S-band
Modulation Format	BPSK
Operating temperature	-40°C to 70°C
Size	0.099x0.094x0.015 m
Weight	0.132 Kg (transmitter) 0.085 Kg (receiver)
Power consumption	13 W
Output power	1 W

**Table 3.6:** ISISPACE S-band transceiver [8]

### 3.1.4 Link budget analysis

The link budget takes into account all the power gains and losses that a communication signal experiences in a telecommunication system, from the transmitter to the receiver. The link budget is a design aid, calculated during the design of a communication system to determine the received power, to ensure that the information is received intelligibly with an adequate signal-to-noise ratio for each of the operations of the TTMTTC subsystem.

#### X-band link budget (downlink)

The link budget for the downlink of the scientific data is carried out by imposing a data rate of 100 Mbps as reported in [4], to calculate the EbN0 ratio and verify that there is a margin greater than 3 dB with respect to the target one, as stated by the ESA philosophy, even in the worst case scenario. The target EbN0 ratio is retrieved by imposing a bit error rate of  $10^{-5}$  and a BPSK modulation. The results are reported below in Table 3.7 and Table 3.8.

$P_{tx}$	1 W		
Distance WCC	734.331 Km		
Modulation	BPSK		
BER	$10^{-5}$		
EIRP	25.456 dB	$EbN0_{target}$	9.6 dB
R	100 Mbps	$EbN0$	33.046 dB
$G_{tx}$	25.52 dB	Margin	23.446
$G_{rx}$	59.496 dB		
$L_{cable}$	-0.06 dB		
$L_{space}$ WCC	-167.929 dB		
N0	-203.977 dB		

**Table 3.8:** X-band link budget downlink results**Table 3.7:** X-band link budget downlink

#### S-band link budget (downlink)

The link budget analysis for the S-band link has been carried out in order to verify if the link margin between the target EbN0 ratio (11.2 dB, retrieved from graphs by imposing a BPSK modulation and Bit Error Rate of  $10^{-7}$ ) is greater than 3 dB with respect to the calculated one with a data rate of 16 kbps as reported in [4]. The results are reported in 3.9 and 3.10.

$P_{tx}$	1 W
Distance WCC	734.331 Km
Modulation	BPSK
BER	$10^{-7}$
EIRP	4.246 dB
R	16 kbps
$G_{tx}$	4.306 dB
$G_{rx}$	48.174 dB
$L_{cable}$	-0.06 dB
$L_{space}$ WCC	-156.608 dB
N0	-203.977 dB

$EbN0_{target}$	11.2 dB
$EbN0$	52.73 dB
Margin	41.53 dB

**Table 3.10:** S-band link budget downlink results**Table 3.9:** S-band link budget downlink

### S-band link budget (uplink)

This link budget is calculated to verify the feasibility of a telecommand uplink for CryoSat. By considering an Equivalent Isotropic Radiation Pattern (EIRP) of 50 dB from the ground stations and a data rate of 4 kbps, the EbN0 ratio is calculated in the worst case scenario: the maximum distance between the transmitter and receiver architectures. The target EbN0 ratio is then retrieved by imposing a Bit Error Rate (BER) of  $10^{-7}$  and a BPSK modulation to check if the margin is greater than 3dB accordingly with ESA philosophy. The results are reported below in Table 3.11 and Table 3.12.

Distance WCC	734.331 Km
Modulation	BPSK
BER	$10^{-7}$
EIRP	50 dB
R	4 kbps
$G_{rx}$	3.902 dB
$L_{cable}$	-0.06 dB
$L_{space}$ WCC	-156.204 dB
N0	-203.977 dB

$EbN0_{target}$	11.2 dB
$EbN0$	60.636 dB
Margin	49.436 dB

**Table 3.12:** S-band link budget downlink results**Table 3.11:** S-band link budget uplink

### 3.1.5 Visibility and Data download

In order to verify when CryoSat is capable to communicate with the Kiruna Ground Station, an analysis of the visibility windows is carried out. The analysis is conducted by the software General Mission Analysis Tool (GMAT) to calculate the visibility of the satellite with the Ground Station. In this analysis the s/c is assumed to be visible when the elevation angle  $\alpha$  is greater than  $5^\circ$ . The mean number of contacts and the mean duration of contacts per day with the Ground Station are reported in Tab.3.13.

Mean # of contacts	Mean Duration of contacts	Propagation
12	1h 34 min	31 days

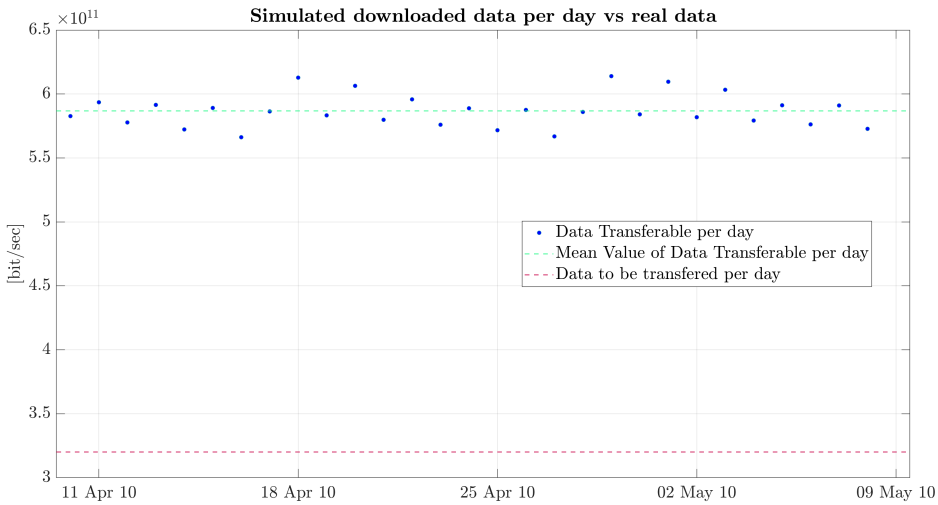
**Table 3.13:** Mean duration and number of contacts

Once the information about the contacts are computed, the analysis of the Data Rate is carried out. The values of the Data Rate and the total amount of downloaded Data, founded in the CryoSat datasheets are shown in Tab.3.14.

Data Rate	100 Mbps
Data volume per day (nominal)	320 Gb

**Table 3.14:** Data Rate and the total amount of downloaded Data

By multiplying the Data Rate by the duration of the contacts, as shown in Fig. 3.3, the total amount of data transferred is computed.

**Fig. 3.3:** Simulated downloaded data per day from 10<sup>th</sup> April 2010 to 8<sup>th</sup> May 2010 compared to the real data

The mean value of the downloaded data is 569 Gb. This value is 1.8 times the nominal one but this result is considered acceptable since transients in the communication links have not been studied and the design has been performed by setting the data rate fixed at 100 Mb/s.

## 3.2 Propulsion System

In this section the analysis on the propulsion system is presented. CryoSat was designed with the idea of avoiding the need for a system to perform any major orbital transfer. This was made possible, as already stated, by having selected a launcher capable of inserting it into its final orbit. As a result, the satellite is not equipped with a proper propulsion system, but rather with a reaction control system (RCS) capable of performing attitude control and orbit maintenance (also referred as AOCS). The reason behind the selection of such architecture and the architecture itself are discussed in the following subsections.

### 3.2.1 Functionalities

Given the profile of the mission, the following functionalities relative to a propulsion system can be identified:

- **F.1.1** Correct launcher injection error
- **F.7.1** Perform orbital maintenance manoeuvres
- **F.7.2** Perform orbital correction when required by the mission control centre
- **F.7.3** Perform collision avoidance manoeuvres when needed
- **F.11.1** Provide information about the tank physical parameters
- **F.11.2** Provide information about the pressure on the feeding lines

### 3.2.2 System Selection

Given the list of functionalities, it is possible to look for the best solution that allows to satisfy them while being compatible with the other mission requirements, configuration of the satellite and cost of the mission.

The first propulsive solution category that is worth discussing is the chemical propulsion. These solutions are capable of exerting high thrust with a relatively low specific impulse. Among them some would be discarded a priori such as solid or hybrid systems for obvious reasons. Liquid propulsion, on the other hand, could be used for this mission profile. Either bi- or monopropellant systems can be installed on a satellite, however such systems shall be pressure fed due to complexity, as pump functioning would interfere with the pointing and be unnecessarily complex.

A second macro category of propulsion systems is the one of electric thrusters. It includes many different solutions all characterised by employing electric energy as primary source and having low thrust over weight ratio, high specific impulse and high dry mass. These systems are more recent and have started to be widely used as primary means for station keeping for geostationary satellites.

Lastly, the presented functionalities can be carried out by a cold gas system which is much cheaper and simpler but has worse performances than the systems belonging to the other two categorises. In the next table (some) of the principal propulsion systems are listed. Their specific impulse values, however, are purely indicative as each specific implementation shows different properties.

Technology	$I_s$ [s]	Advantages	Disadvantages
Monopropellant	150÷225	Only one propellant is needed. Storable propellant exist.	High power required to heat the catalyst. Weight and cost of the catalyst.
Bipropellant	200÷300	High thrust and good specific impulse.	High complexity and lower reliability.
Cold Gas Thrusters	50÷100	Simple, reliable and cheap system.	Low specific impulse means more propellant needed.
Resistojet	200÷300	High thrust (among the electric systems). May use any propellant	Relatively low power required. Thrust obtained from thermodynamic expansion.
Arcjet	400÷800	Low voltage required.	Power required $\sim 1\text{kW}$ . High losses due to gas dissociation.
Ion propulsion	1500÷5000	Very high specific impulse. High efficiency	Power required $\sim 1\text{kW}$ . Grid Erosion.
Hall thruster	1500÷2000	High specific impulse. Use of inert propellant.	Beam divergence. Erosion.
Solid pulsed plasma	600÷2000	Relatively simple. Uses solid propellant cartridge, no need for feeding systems or tanks.	Low propulsive efficiency. Contamination. No continuous thrust. Very small thrust.

Table 3.15: Propulsion technologies comparison[9]

From table 3.15 it is possible to deduce that there are some desirable properties in different solutions. Indeed the ideal propulsion system would have:

- The high specific impulse of an electric system to use as little propellant as possible.
- The low power consumption of a chemical system to be operated without the need to turn off other systems, to oversize the power supply system or to have a dedicated power control unit.

- The simplicity of a solid pulsed plasma system which can use storable solid cartridges without the need for any feeding system or tank.

The designers of CryoSat, however, opted for a reaction system based on cold gas thrusters. The likely reasons for this selection are:

- Reduced cost
- Reliability
- Established technology
- No reactive chemical substances required, which made the production process safe and cheap.
- No heating involved, hence no need for thermal insulation.
- Low thrust, which make it possible to use the very same system to also control the attitude by using just two nozzle geometries.
- Low power required, which made it possible to manoeuvre even in eclipse and made unnecessary a complex power regulator.

That being said, this selection had drawbacks as well, indeed the extremely low specific impulse make it a limiting factor for the mission duration since any station keeping manoeuvre requires more propellant than with any amongst the other solutions presented before. This gives the chance to praise the optimization and the planning of the orbit maintenance manoeuvres which have allowed CryoSat to be still operative some 9 years past its design life. As a case study the orbit raising manoeuvre performed by CryoSat in 2020 is compared in terms of cost and duration for the actual system and a similar ion thruster system in the Appendix C and would serve as additional justification of the design choice made.

### 3.2.3 Reaction Control System Configuration

CryoSat's RCS architecture is relatively simple, it consists in: a High-Pressure storage tank, mechanical pressure regulators, and Low-Pressure thrusters. The selected propellant was Nitrogen ( $N_2$ ).

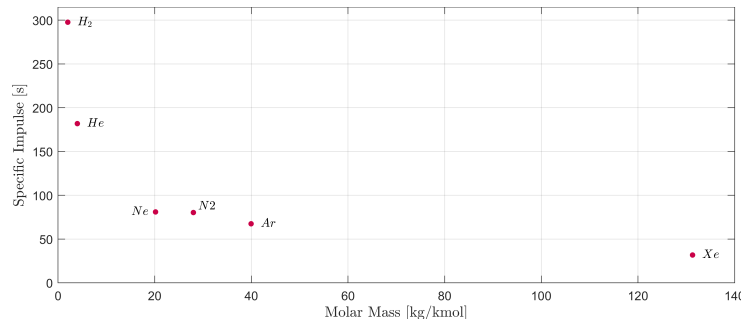


**Fig. 3.4:** Comparison of the specific impulses for the most common operating gases.

The specific impulse guaranteed by nitrogen is 72s circa, as stated by the technical reports of the system, and confirmed in the plot above. The selection of nitrogen did not guarantee a specific impulse as high as the one of hydrogen or helium but, being denser, allowed to limit the occupied volume. The selection of nitrogen is moreover a very common one given the production cost, availability and the inertness of the gas.

Due to the use of the RCS as auxiliary actuator for the Attitude and Orbit Control System (AOCS) it was equipped with a large number of nozzles. The spacecraft carries 16 Attitude Control Thrusters (ACTs) and 4 Orbit Control Thrusters (OCTs) with a thrust level of, respectively 10 and 40mN apiece, organized in two redundant branches of 2 OCTs and 8 ACTs. The power

consumption of the system can be estimated by comparing it with some alternatives present on the market. They allow to estimate a power consumption  $\sim 10W$  per thruster [22]. Figure 3.5 shows the position of the ACT and the OCT within the spacecraft.

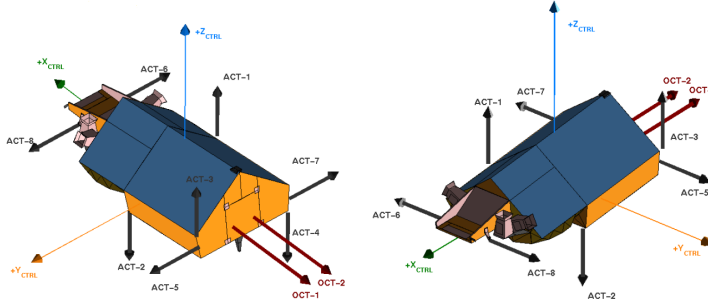


**Fig. 3.5:** Accommodation of the attitude/orbit control thrusters. (ACT/OCT)

The sole difference between the two thrusters is in the throat diameter, which affects the thrust generated and the mass-flow demand. The attitude-control thrusters' design imposed no ACT thrusters oriented in the along-track direction, i.e. along the spacecraft Roll axis, due to accurate orbit determination requirements. Of the 8 ACT, half of them are used for Yaw control, the others for the combined Roll-Pitch control, as it can be deduced from their positions. These are operated in a pulsed manner with variable pulse duration from 50 ms to 10 seconds. The OCT are all positioned on the same face of the satellite along the Roll axis, to minimize torque when active. They are operated in a continuous manner.

### 3.2.4 System Architecture

The aim of this chapter is to present more in detail the architecture of the propulsive system of CryoSat, all the information here reported can be traced to [23]. The propellant, 36.7 Kg at beginning of life, is held as a high-pressure gas (278.6 bar at BOL) in a single spherical tank and then flows through a single-stage Pressure Regulator (PR), where the upstream pressure is decreased to a constant low pressure of roughly 1.3 bar with a flow rate up to 0.25 g/s..

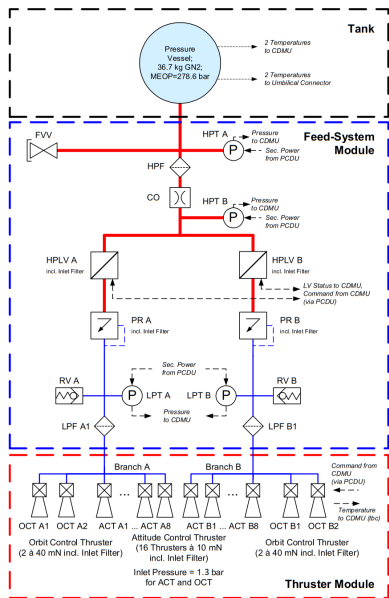


**Fig. 3.6:** Propulsion System Schematic

The regulator stays in the lock-up position until the system initiates a flow demand (by means of a commanded opening of the thrusters). Depending on the number and kind of actuated thrusters, the outlet pressure falls when a flow demand from the downstream system arises. The architecture of the system is portrayed in the figure on the left. The main elements that can be immediately observed are:

- Tank
- Feeding lines
- Valves
- Nozzles

From the figure it is also possible to observe the telemetry performed by the system.

**Tank** The relevant data of the tank can be deduced from figure 3.6, then the volume that the

tank shall have can be deduced. For the calculations, a 5% uncertainty on the computed internal volume is taken into account. Two shapes were considered: a cylindrical tank and a spherical tank in order to understand which is best. As a result, the spherical tank internal radius was found to be 30.6 cm. While for a cylindrical tank with a length over radius ratio of 2 (arbitrary value), the radius is 22.7cm and the total length of 90.8 cm. For the sizing, the burst pressure was fixed adding a 50% margin to the maximum working pressure. Having fully defined the geometry, the following values of weight were computed for different materials:

Material	Spherical mass [kg]	Cylindrical mass [kg]
Aluminium	43.75	53.21
Titanium	22.70	27.44
Steel	37.65	43.38
Carbon fiber	5.70	6.86

Table 3.16: Tank weight comparison

From similar missions it is highly likely that titanium was selected as material. As already said, the ratio between length and radius of the cylinder was arbitrarily fixed. However, multiple weight computations with different values for the ratio were done in order to see how the weight evolve with the length. The results are reported in the following chart:

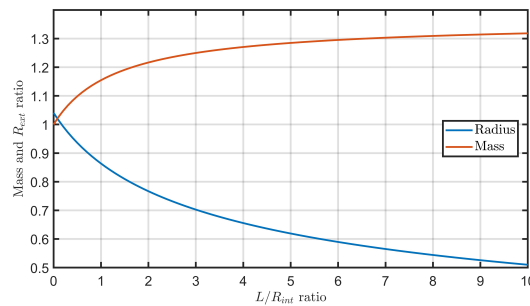


Fig. 3.7: Mass and external radius ratio between cylindrical and spherical tanks vs slenderness ratio for the same internal volume.

It allows to conclude that the slender the cylindrical tank, the higher its mass compared to the spherical alternative despite this makes its shape more efficient to pack within the satellite. That being said the decision of a spherical tank can be motivated by the decision to contain the weight.

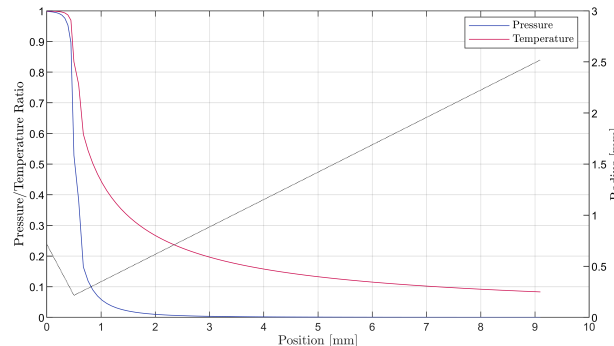
Lastly, the centre of mass of the satellite is located at the centre of the only spherical tank. This decision is clearly motivated by the need to preserve the mass distribution during the lifetime of the satellite, and to avoid the need to adapt the attitude control authority to the changes of the attitude matrix.

**Feed-system module** The system presents two parallel lines, they are completely identical, for redundancy. In nominal condition only one is kept operative. Only for exceptionally demanding manoeuvres the system can operate them both. The following elements can be identified:

Component	Purpose
Fill Vent Valve (FVV)	Regulate filling and discharge of the tank
High Pressure Transducer (HTP)	Monitoring of the pressure on the line
High (Low) Pressure Filter (HPF/LPF)	Prevent particles from proceeding along the feeding line
Control Orifice (CO)	Limit the flow in the event of a pressure regulator fails to open
Latch Valve (HPLV)	Provide the means for isolating the high pressure supply from its low pressure section
Pressure regulator (PR)	Regulate the pressure in the line
Relief Valve (RV)	Avoid damage due to overpressure

**Table 3.17:** Feed-System Module components

**Nozzles** As mentioned before, the reaction system employs two different nozzles. Their shape is the same but for the throat area. The OCT have a throat area of 0.43 mm, (0.22 mm for the ACT), a length of the divergent part of 8.6 mm and an exit diameter equal to 4.6 mm. The divergent part has a conic geometry with 15° of aperture angle. This detail makes the 2D losses higher than with a bell-shaped one. For the considered case the reduction of thrust is less than 0.5%. In the upcoming Figure 3.8, the pressure and temperature ratios along the axis of the nozzle are plotted. From which it is possible to conclude that the exit pressure is 21 Pa and, assuming an initial temperature of 25°, an exit temperature of 25 K.

**Fig. 3.8:** Pressure ratio along the axis of the OCT nozzle

### 3.3 Attitude Determination and Control System

Being CryoSat an Earth observation mission it is trivial to say that the need to correctly point the ground is of outmost importance. The scientific payload is not however the only one with specific pointing requirement. CryoSat's configuration, however, put together these potentially different requirement allowing the satellite to be always nadir pointing without the need to change the attitude to perform different activities.

#### 3.3.1 Functionalities

According to the mission the following functionalities can be deduced:

- **F.4.1** Perform the detumbling after the release
- **F.4.2** Determine the current attitude
- **F.4.3** Control the attitude of the satellite
- **F.4.4** Correct pointing errors
- **F.4.5** Adapt the operational mode to the mission status

### 3.3.2 System Definition

In order to justify the adopted architecture of the ADCS is necessary to look at the payload's requirement. From what has been discussed in the previous chapter of this report, the most demanding measurement mode occurs when SIRAL is operated in SARin mode. Operating in this mode requires a pointing accuracy better than  $0.2^\circ$ , and high pointing stability, the X-band antenna used for scientific data download requires instead a control accuracy better than  $4^\circ$ . The requirement and budget found in the literature are[24] [4]:

Quantity	Control Accuracy	Pointing Knowledge	Stability over 0.5s
Requirement	$<0.2^\circ$	$<35''$	$<0.005^\circ$
Budget Value	$0.1^\circ$	$27.6''$	$<0.001^\circ$

**Table 3.18:** Pointing Requirements

Such strict requirements left no other options but to adopt a three-axis stabilization architecture for the satellite, in order to be able to completely control the attitude. The requirement on the pointing accuracy and the higher value on the knowledge requirement impose the need for very accurate actuators and sensors. One additional important remark is that, in order to preserve as much as possible the stability of the pointing, the presence of moving mechanisms on board shall be as limited as possible. Lastly, the satellite flies in a "nose-down" attitude, inclined by  $6^\circ$ , in order to avoid excess torques due to gravity gradient effects. This allowed to save energy to compensate for this, otherwise constant, disturbance.

### 3.3.3 Sensors Description

The ADCS relies on a series of different devices to retrieve information about the attitude and rates of the platform. The data gathered by the sensor are elaborated by the CDMU since no dedicated processor exists. This decision was likely made to reduce the cost.

**Star Trackers (ST)** The presence of this instruments could have been foreseen given the high accuracy knowledge requirement. These are sometimes considered as part of the payload since, like DORIS, they help locating the satellite in its orbit contextualising the SIRAL measurements. There are three autonomous devices positioned in the antenna bench of the platform to maximize the stability between them and the antennas frame of SIRAL. The configuration is one-failure tolerant except for the occurrence of simultaneous Sun and Moon blinding of the remaining two (if that is the case the system will shift to coarse pointing mode), their FOV is  $22^\circ \times 22^\circ$ . When operating nominally, they provide information about the attitude with a frequency of 1.7 Hz. The software does compensate for cosmic rays entering the FOV and electrically charging a pixel in the CCD which could be mistaken as a star [25].

**Coarse Earth and Sun Sensor (CESS)** This sensor is less accurate than the previous one and is mostly used in coarse pointing mode or safe mode. The field of view of the sensor is spherical. It consists of 6 sensor heads arranged in all 3 orthogonal directions where the shadows projected by the satellite's elements are minimized. Each head, with known optical properties measure a temperature, from the temperature distribution the software deduces the position of the Sun and the Earth. The measurements are provided with 1 Hz frequency. The instrument is internally hot redundant.

**Fluxgate Magnetometers** Three hot redundant magnetometers, located in the nose of the satellite (opposite to the magnetotorquers) are used as rate sensors and for magnetotorquer control. Majority voting of the three outputs makes the system one-failure tolerant.

**Experimental Rate Sensor** This device is an attitude rate sensor based on Micro-Electro-Mechanical-System (MEMS) technology. It detects the attitude providing the same kind of information of a traditional gyro. The data it produces, however, are not used on-board, but are directly sent on ground to monitor the satellite dynamics.

The power consumption of the reported instruments can be estimated by analyzing the consumption of similarly performing devices available on the market, an approximated value of 25 W (without margins) can be assumed.

### 3.3.4 Disturbances Analysis and Actuators Selection

A simplified model of the satellite (uniform mass distribution and simplified geometry) was considered to evaluate the environmental disturbances torques acting on the satellite, considered with the nominal (nadir pointing) attitude. The results obtained for two orbits are shown in the next figure:

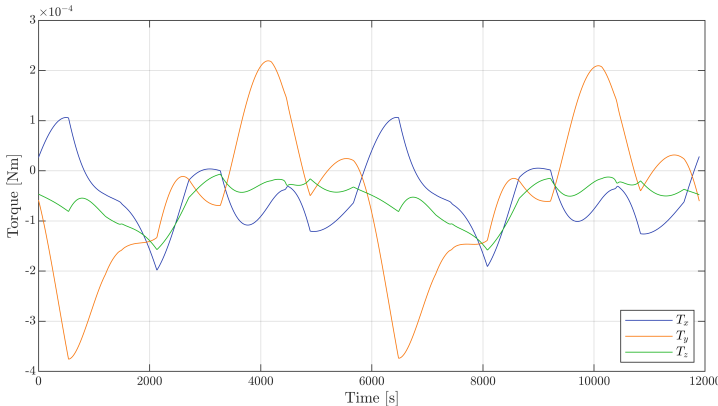


**Fig. 3.9:** Sum of Environment disturbance torques in body axes

From [24], however, the highest torque is considered to be the magnetic one. This may be due to the simplifications made in defining the model of the satellite, and on the fact that its residual dipole moment was assumed from [26] for a class II satellite. As expected, SRP and the magnetic torque acted on a periodic way while the others were more or less constant during the orbital period. Environmental disturbances are not the only one affecting the attitude of the satellite. The internal sources were, however, deemed to be not influential in the identification of the actuator technology. In the satellite there are no liquid on board, almost no moving parts are present and, because of the position of the tank, the centre of mass has moved to the date of this writing of only one millimeter along the roll axis[27]. The latter has been deemed negligible.

That being said the designers opted for 3 internal redundant (redundant coils on a single rod) magnetotorquers and a set of ACT (already described in the section devoted to the propulsion system). The reason of this selection are listed below:

- The need to reduce as much as possible the internal disturbances and by extension the moving parts has lead to the exclusion of momentum exchange devices.
- The low altitude of the orbit suggested the possibility to exploit the strong magnetic field to orient the satellite.
- The contemporary need for a propulsive system suggested the possibility to merge in a single architecture the orbital and attitude control functions.

**Magnetotorquers (MT)** Three devices, oriented in parallel with the reference axes of the satellite, are positioned in the aft of the platform (far from the magnetometers) and are characterized by a low residual dipole moment. Their moment dipole is  $\pm 30 \text{ Am}^2$ [24]. To understand why such actuators have been selected the moment dipole required to these actuators to instantaneously compensating the sum of the disturbances was computed, after applying a 100% margin on their value.

The considered disturbances are, in the expected decreasing order of intensity:

- SRP
- Gravity Gradient
- Magnetic Field Torque
- Drag

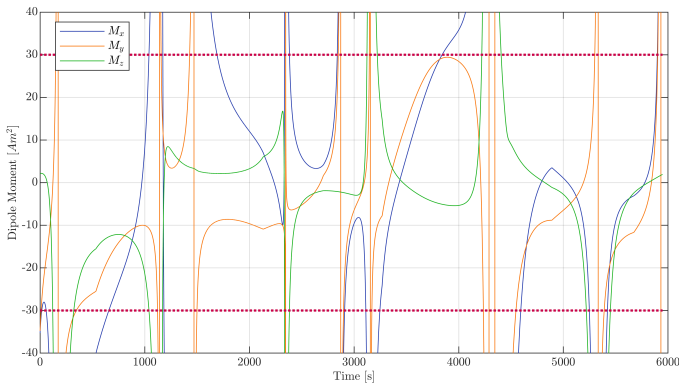


**Fig. 3.10:** Required moment dipole to compensate the disturbances

**Attitude Control Thrusters (ACT)** They have been already introduced when talking about the reaction control system, thus a complete description is here avoided. They have been deemed more than capable to compensate for the disturbances computed with the employed model. Indeed, considering the worst condition: the maximum torque is  $\sim 10^{-4} \text{Nm}$  and is about the roll axis while the exerted torque is  $\sim 10^{-2} \text{Nm}$ , with the employed actuators. No time critical manoeuvre are forecast during the nominal life of the satellite (such as epoch specific pointing change). Therefore any attitude change, as may be needed immediately before and after the orbital maintenance manoeuvre may be performed without strict time requirements. Therefore the actuators currently present are deemed sufficient, as they can exert a control authority always higher than the disturbances.

The power consumption for the attitude control is estimated, under nominal condition to be less than 50W (without margins), of which 4.5W are needed by the MT and 40W by four ACTs[22].

### 3.3.5 Modes

From the analysis of the mission phases one can deduce that the number of pointing modes is limited by the fact that there is only one direction to be pointed: the ground. Thus no slew manoeuvre mode can be assumed for CryoSat. The literature [28] [24] identifies five control modes:

- **Stand-By Mode:** Purely passive mode initiated after launcher separation or after any reboot of the system. It performs the necessary initialization, never repeated.
- **Rate Damping Mode:** Executed when it is necessary to reduce the satellite angular velocity such as after the deployment (detumbling) or whenever necessary. Both magnetic torquers and ACT are used. After the system has been rebooted according to a timelined procedure the RDM is initiated. It applies proportional gains to generate torque demands for the ACT and MT. Initial rate of  $3^\circ/\text{s}$  are damped below  $0.1^\circ/\text{s}$  in 72 minutes circa[24], then as the angular rate decreases and the CESS becomes available the mode shifts to the CPM.
- **Coarse Pointing Mode:** The CESS is the primary attitude sensor, ACT are used to guarantee a pointing accuracy of  $15^\circ$  (sufficient to guarantee power production and S-band communications), the pointing knowledge is in this case lower than  $6^\circ$ [24]. This mode coincides with the safe mode, the payload is turned off, the telecommunications occur with the omnidirectional S-band antenna.
- **Fine Pointing Mode** This is the normal operating mode kept for most of the mission. The high performances portrayed in Tab.3.18: are obtained by using the star trackers and maneuvering mostly with the MT, using the ACT to cover high demands.
- **Orbit Control Mode:** Necessary to prepare the satellite for orbit changes and maintenance maneuvers.

The required values diverge when the external magnetic field crosses the zero value. However, the installed actuators are deemed sufficient as these events are transitory. Eventual inabilities of the MT to supply sufficient torques can be compensated by the use of the ACT.

This can be translated in the following logical scheme:

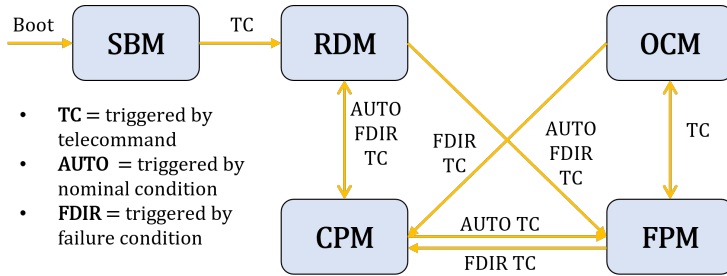


**Fig. 3.11:** ADCS control logic scheme

## 3.4 Electric Power System

The EPS is in charge to generate, store, control and distribute the electric power over the whole s/c. In this section the EPS of CryoSat will be deeply analyzed starting from the functionalities and the related requirements. The system will be then re-designed in order to justify the adopted architecture and to analyze the inputs and constraints imposed to the other subsystems present on-board.

### 3.4.1 Functionalities

Before going into the architectural details, the first step needed for a proper understanding of the subsystem is to set the functionalities and requirements. Generally speaking, an electric power system should perform the following tasks:

- **F.8.1** Supply a continuous and sufficient power amount to the satellite
- **F.8.2** Control and distribute the electrical power to each system
- **F.11.3** Measure battery temperature and capacity
- **F.11.4** Measure power production level

Then we can define the related requirements the EPS will have to satisfy and they are listed in F.7.

### 3.4.2 Power source selection

The CryoSat mission takes place in the Low Earth Orbit (LEO) region at a mean altitude of 720 Km for an estimated lifetime of 3.5 years (later on the mission lifetime has been extended after the primary objectives have been completed).

Accordingly to the graphs in Figure 3.12, as primary source of electrical power for Cryosat, photovoltaic is a suitable choice. This is in line with many other LEO applications thanks to the proximity to the Sun and its embedded renewable nature. Moreover, to help the solar array satisfying peak power demands and allow the spacecraft to be operational also during eclipse phases, a secondary battery pack has been included. The couple solar panel and secondary battery is widely adopted among spacecrafsts, making it a trusted and almost off-the-shelf ready technology.

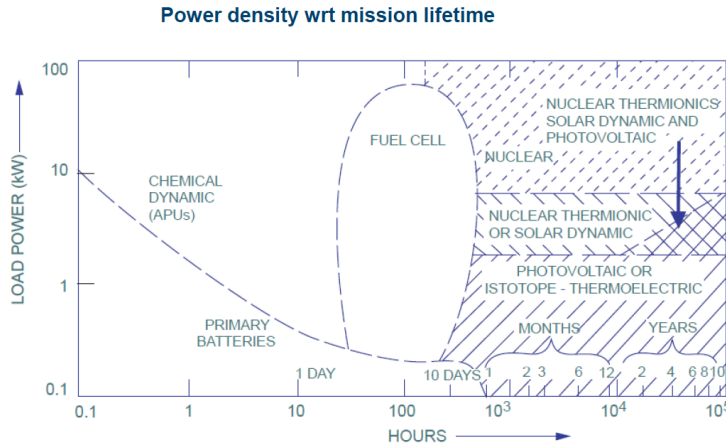


Fig. 3.12: Power source alternatives and taxonomy

### 3.4.3 Power budget breakdown

Once the qualitative key points have been set, in order to start a proper analysis and design of the EPS some quantitative considerations need to be performed. The pivotal one consists in defining the power budget that the spacecraft will require in each phase and mode in which it will operate. Data found in literature and reported in Table 3.19 shows that the Worst Case Condition (WCC) in terms of power absorption occurs when Cryosat is in its scientific phase with SIRAL operating in SAR mode (Synthetic Aperture Radar) while downloading the scientific data by means of the X-band antenna.

Item	SIRAL Standby	SIRAL LRM	SIRAL SARIn	SIRAL SAR	SIRAL SAR + X-Band
SIRAL	61.9	95.6	124.1	127.1	127.1
DORIS	30.0	30.0	30.0	30.0	30.0
Platform	188.5	189.7	191.4	182.6	264.4
Satellite	281.9	317.5	348.3	342.4	425.9

These values do not include margins nor the power required for battery charging. Satellite value includes dissipation in wiring harness.

Table 3.19: CryoSat nominal power demand for different modes[4].

The next step consists in defining at a subsystem and component level the electrical power required for the identified most demanding mode, in which all components have been assumed active. Specifically the ADCS will be working for sure because the SIRAL SAR mode requires an accurate pointing. Table 3.20 summarizes the power demand for the subsystems studied so far and compares them with average statistical values found in other LEO space crafts. It should be noted that no electrical power was counted for the battery charge in order to have a consistent comparison with the values found from official literature in Table 3.19.

ITEM	NOMINAL POWER [W] (MARGINS)	% TOTAL POWER	AVERAGE STATISTICS	CRYOSAT PAPERS[W]
<b>PAYOUTLOAD</b>		36.9%	40-45%	
SIRAL***	127.5 (153)			127.1
DORIS*	20(21) nominal 30(31.5) warm up			30
<b>TTMTC</b>		6.6%	10-15%	N/A
X-band transmitter*	15 (15.75)			
S-band transceiver*	13 (13.65)			
<b>AOCS</b>		21.1%	10-20%	N/A
Star trackers*	21 (22)			
Magnetometers*	4.5 (4.7)			
Coarse Sun sensor	passive			
Exp. rate sensor***	0.1 (0.12)			
Magnetotorquers*	4.5 (4.7)			
Cold gas thrusters*	60 (63)			
<b>CDH</b>		~ 0%	10-15%	N/A
Processor* (E.3)	1 (1.05)			
<b>EPS</b>		-	10%	N/A
Battery	-			
Solar array	-			
<b>TCS</b>		7.3%	5-10%	N/A
Heaters* (3.5.3)	25 (31.25)			
Total	340.7 (margins) 408.8 (extra 20%)			425.9 511.08 (+ 20%)

\* +5% margin (Category A-B product); \*\* +10% margin (Category C product); \*\*\* +20% margin (Category D product); Additional 20% margin at system level

**Table 3.20:** CryoSat power budget breakdown

It is now worth making a couple of comments on the resulting power budget breakdown. While concerning the Payload the values found are coherent with the actual implementation, the TTMTC subsystem appears to be underestimated; that is because our re-design has been done to just met the minimal performance requirements whereas the real system may have been sized differently. On the other hand the AOCS power requirement slightly exceeds the average statistics for LEO satellites but it is reasonable since the operating mode under analysis requires an extremely accurate pointing of the instruments. Lastly the OBDH results do not influence at all the spacecraft power demand. This is because in Appendix E only the processor design has been made and it represents just a small portion of the entire subsystem.

### 3.4.4 Primary power source sizing - SA

In this section the design of the solar arrays is conducted in order to compare the result with the real architecture present in CryoSat. The starting point is the required power analysed during the power budget breakdown to finally compute, at the end of the design process, the mass and area of solar arrays.

By looking at Table 3.20 it is possible to notice the difference between the computed power required and the one retrieved from the literature. Such a discrepancy is due to the fact that our value has been computed by summing the power consumption of the devices that have been selected during re-design processes; therefore they are not fully representative of the power consumption of the actual subsystems. Specifically it can be thought that while our re-design process was conducted in order to met only minimal requirements, as in the TTMTC case, real components might have

been slightly oversized as consequence of design iterations. At last it has been enhanced the presence of missing values for subsystems that are still to be considered.

Concerning the choice for the baseline power level, in [10] it is clearly stated that the solar panels have been designed to provide a maximum power of 880 W (which approximately corresponds to 106% of margin instead of the usual 20% to allow nominal operations even in case of shadowing of one of the panels). Consequently, in order to critically compare the design results such value has been taken as starting design parameter.

The mentioned oversized margin has made possible to minimize the Depth of Discharge of the batteries and to keep their charge/discharge rate under conservative limits, ensuring a longer operational lifetime without need of a strict battery control and management. For this reason, the EPS s/s has been capable to sustain the extension of the mission duration after CryoSat completed the main mission objectives.

The total power required by the solar panels has been retrieved by considering the power demand of the s/c during eclipse ( $P_e$ ) and daylight ( $P_d$ ) phases in the worst case condition, applying respectively an efficiency factor  $X_e = 0.65$  and  $X_d = 0.85$ . As already studied in the mission analysis chapter and reported in Fig. 2.1, the maximum eclipse duration can be estimated as  $T_e = 36.7$  minutes. The corresponding shortest sunlight time is therefore  $T_d = 62.4$  minutes.

Then, the power produced at beginning-of-life  $P_{BOL}$  has been calculated by taking into account an efficiency  $\eta_{3J} = 27.5\%$  for triple-junction Ga-As solar cells, an advanced technology at the time of design, and an inherent degradation factor  $I_d = 0.6$ . The power produced at the end-of-life  $P_{EOL}$  has then been computed introducing a degradation factor  $L_d$  which considered a lifetime of 3.5 and 5.5 years (The last value has been taken into account to evaluate the possibility of extension of the mission). Finally, the area and the mass of the solar panels have been obtained considering a specific power  $P_{spec} = 80 \text{ W/Kg}$ .

### Sizing results - SA

The comparison between the obtained results and the real architecture is presented in Table 3.21

-	$P_r$ [W]	A [ $m^2$ ]
Real architecture	880 W	9.2 $m^2$
Re-design (3.5 years)	880 W	9.348 $m^2$
Re-design (5.5 years)	880 W	10.091 $m^2$

**Table 3.21:** Results comparison

Specifications of the on-board solar array are presented in Table 3.22 below.

-	Description
Solar array type	Body fixed design, no deployment mechanism required
Cell type	Triple junction Ga-As
Cell efficiency	27.5%
Cell size	40 mm x 80 mm x 160 micron
N° of sections	11 per panel
Mass	26.165 Kg (calculated)
Operating temperature	From -170° to 145°

**Table 3.22:** Solar array specifications [10]

The results obtained can be considered acceptable with respect to the real architecture, in particular since the margins taken into account are very wide the 3.5 years solution is deemed to be the best alternative. The mass, area and operating temperature are parameters that impose constraints over other subsystems; specifically mass and area have a link with the structural subsystem and the spacecraft geometry, while temperature will affect the TCS.

### 3.4.5 Secondary power source sizing - Battery

In this section a re-design of the battery pack is performed in order to compare the results with the real architecture. As a starting point the required energy  $E_r$  of the battery has been computed by exploiting the power needed during eclipse phases  $P_e$  and the time  $T_e$  (which represents the worst case condition of eclipse). As done for the solar array sizing, the power  $P_e$  has been taken equal to 880 W. Such a high margin have been used also for the battery because it ensures that the secondary power source will be able to satisfy the peak power request, which is hard to be estimated, even in full eclipse conditions. In addition to that, this value ensures that in case of failure of some internal battery cells the spacecraft operations will not be compromised. Lastly, this design choice allowed the CryoSat mission to be extended much more than the possible 5.5 years targeted lifetime because a better battery management had been made possible improving their expected operational time.

The total capacity required for the battery design is retrieved by considering an efficiency  $\eta_b = 95\%$  and the Depth of Discharge (DoD) which was computed as 30% for a 3.5 years mission lifetime and 25% for a 5.5 years mission. By performing this analysis it's possible to verify the feasibility for a mission extension. Finally, by considering the energy density per unit mass  $E_d = 150 \text{ Wh/Kg}$  and energy density per unit volume  $E_v = 200 \text{ Wh/dm}^3$  the total mass and volume of the battery pack has been retrieved. The s-p topology of the battery cell has been designed starting from the total capacity  $C_{Ah} = 67.452 \text{ Ah}$  for a 3.5 years mission and  $C_{Ah} = 80.942 \text{ Ah}$  for a 5.5 years mission and the interface voltage  $V = 28 \text{ V}$  considering a capacity  $C_{cell} = 1.5 \text{ Ah/cell}$  and voltage  $V_{cell} = 3.7 \text{ V/cell}$  [11].

#### Sizing results - Battery

The comparison between the obtained results and the real architecture are presented in Table 3.23

-	$C_{Ah}$	Topology
Real architecture	78 Ah	8 serial cells in 52 parallel strings
Re-design (3.5 years)	67.452 Ah	8 serial cells in 45 parallel strings
Re-design (5.5 years)	80.942 Ah	8 serial cells in 54 parallel strings

**Table 3.23:** Results comparison

The specifications of the battery are presented in Table 3.24 below.

-	Description
Battery type	Li-Ion
Efficiency	95%
DoD (3.5 years)	30%
DoD (5.5 years)	25%
Mass	12.591 Kg (calculated)
Volume	9.44 dm <sup>3</sup> (calculated)
Operating temperature	From -10° to 40°

**Table 3.24:** Battery specifications [11]

The results obtained can be considered acceptable with respect to the real architecture. The mass, volume and operating temperature are parameters that impose constraints over other subsystems; as stated above mass and volume will influence the structural subsystem and the spacecraft geometry, whereas the battery temperature is an important design parameter for the Thermal Control System. Additionally the battery should also be managed by means of the PCDU in order to limit its DoD and be able to work during the whole spacecraft lifetime.

### 3.4.6 Conclusions

The last consideration about the EPS subsystem concerns the Power Control and Distribution Unit (PCDU) which has been designed to interconnect, manage and transform the power sourced by the primary solar arrays and provide it to the loads, allowing to switch on and off each channel while returning their telemetry. Data from official documentations are quite lacking; still a couple of thoughts can be made in order to provide a feasible architecture design. Given the limited amount of power of the spacecraft and its relative simplicity it can be thought that the primary energy source might be controlled just by a passive sequential switching shunt regulator (SSSR). It means that the SA voltage would be kept constant and exceeding generated current is thermally dissipated. Moreover the energy bus can be designed to work at the nominal voltage of 28V DC, which is almost the standard for CryoSat-like satellites. The consequence is that active control on the voltage is required just on the battery side, which are characterized by a change in operating voltage while charging or discharging. Such a design choice would allow to keep the subsystem as simple as possible and use already existing and trusted technology.

Eventually also a couple of observations on the actual architecture and configuration of the energy sources can be made. The area of the solar array is low enough to be mounted on the side of the s/c which will be zenith-oriented during operational activities, without introducing any moving part such as deployment mechanisms which are failure susceptible parts. The panels are covered with Triple Junction Ga-As solar cells, chosen to provide a high efficiency, and are divided in two different parts with an angle of 104° between them. The resulting design is compact, has a low level of complexity, is capable to fulfill all the mission objectives at any local hour of the orbit and it does not introduce problem related to the accommodation in the launcher fairing. The energy is stored by a 78 Ah battery through an array of 1.5 Ah Li-Ion cells during daylight phases in order to provide the electrical power during eclipses and to satisfy peak power demands at EOL.

## 3.5 Thermal Control System

This section contains the result of the analysis of the thermal control system designed for CryoSat. Firstly a brief evaluation of the desirable temperature range will be presented, then the multinodal analysis results will be reported as a confirmation of the mission feasibility from the thermal point of view. The available literature reports that CryoSat thermal environment is kept within the acceptable range mostly by passive means. Only some heaters, controlled by the CDMU, are present.

### 3.5.1 Functionalities

- **F.10.1** Maintain a suitable thermal environment inside the platform
- **F.10.2** Protect from thermal related damages
- **F.10.3** Adapt autonomously to the thermal conditions

### 3.5.2 Temperature Range

In order to fulfill the first functionality it is imperative to determine what is the range of tolerable temperatures for any of the embarked devices. Such range differs between components and depends on the functioning state of the item: the operative limits are indeed narrower than the non-operative ones, which in turn are stricter than the survivable temperatures. For sake of simplicity in the upcoming table only the first are considered. It is worth specifying that exiting from them does not impact the functionalities of the instrument but may affect its performances, as long as the non operating range is respected. Furthermore, such a list does not claim to be

exhaustive nor exact as some of these values were retrieved from items just similar to those actually present on CryoSat.

Item	Battery	SA	X-band A.	S-band A.	SIRAL	Star T.	CDMU
$T_{max}$ [°C]	40	120	100	90	50	70	125
$T_{min}$ [°C]	-10	-140	-120	-80	-40	-40	-55

Table 3.25: Operative Temperature Ranges

From this investigation the batteries turned out being the most sensitive items present on board. The real temperature range of each electronic component present on the platform was not retrieved given the lack of data, but it is safe to assume that theirs were more forgiving.

### 3.5.3 Thermal Analysis

CryoSat is not expected to change much its orbit throughout its life. Being confined in a polar LEO, the following heat sources/sinks can be easily identified: Sun's radiation, Earth's albedo and IR emission and free space (always acting as a sink with a temperature of 2.7 K). The satellite has been modelled through a multinodal approach. Each node corresponds to one of the main 5 lateral surfaces in with the satellite can be approximated and leads from the radiative view point to a pentagonal empty prism without bases; the corresponding view factors have been estimated according to an online tool.

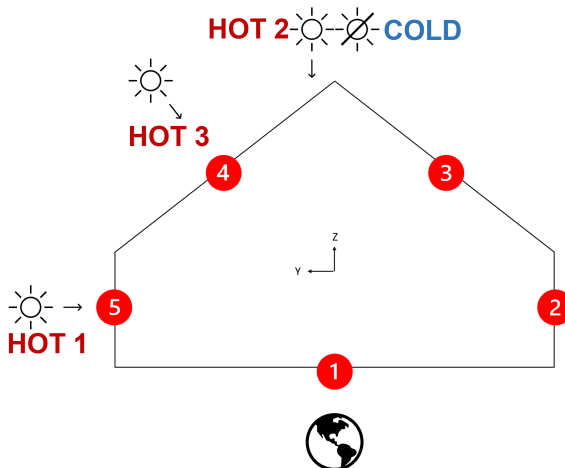


Fig. 3.13: Multinodal Model and Cases

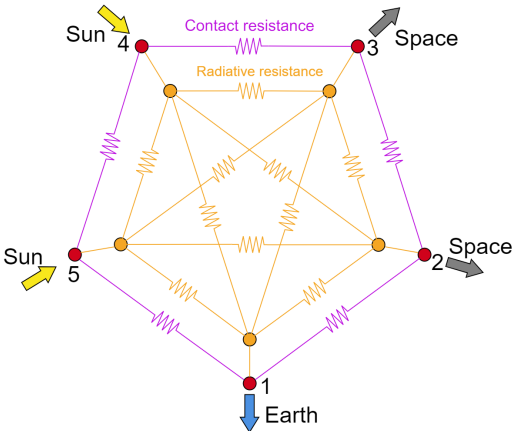


Fig. 3.14: Equivalent thermal circuit.

The masses have been distributed in an unevenly way to account for the fact that most of the internal items, in particular payload, batteries and electronics are attached to the bottom surface (node 1). The results of this analysis are not expected to respect the real ones as each surface was considered optically homogeneous, besides not corresponding exactly to the real one in terms of geometry and size (taken larger to compensate the lack of the bases and the nose). Up to 15 K difference from the real surface value should be accounted, as this is a very preliminary analysis. Hence, the effective temperature ranges are tighter than operative ones: for node 1 it's [5;25]°C (dictated by the battery), for nodes 3 and 4 it should be [-25, 55]°C (dictated by the star trackers), while the remaining nodes were considered as structural and no range has been specified. A total of five analysis have been performed according to the logic of Figure 3.13: one cold case in which the satellite is in eclipse, three hot cases which considered different relative positions between the sun and the z-axis (due to the different RAAN rate of the sun and of the satellite they correspond to a  $\beta$  angle of 90°, 0° and 38°) and a final dynamic analysis of the temperatures oscillations experienced by the satellite when the sun direction lies on the orbital plane (and therefore the eclipses duration is maximized). The last one is actually more meaningful than the cold and second hot cases as the asymptotic temperatures would never be reached because of the excessive

time they require to be met. All these conditions are periodically experienced by the satellite in its nominal orbit without any explicit distinction among the phases or modes of the mission. The results of the analysis are reported in the next table:

	<b>COLD [°C]</b>	<b>HOT 1 [°C]</b>	<b>HOT 2 [°C]</b>	<b>HOT 3 [°C]</b>	<b>DYN [°C]</b>
<b>Node 1</b>	-106.39	2.52	24.59	20.40	[2.73; -3.01]
<b>Node 2</b>	-114.40	-14.05	34.97	13.94	[22.67; -27.82]
<b>Node 3</b>	-121.35	-21.26	66.13	22.45	[61.62; -52.43]
<b>Node 4</b>	-121.35	21.40	66.13	72.00	[61.62; -52.43]
<b>Node 5</b>	-114.40	28.15	34.97	43.53	[22.67; -27.82]

**Table 3.26:** Multinodal Thermal Analysis Results

The results contained by the static cases represent the equilibrium temperatures of each node while the last one contains the oscillation ranges. The plots, obtained for an initial temperature of 25° are reported in the Appendix D. From the obtained results the following considerations have been made:

- Due to the orbit orientation the satellite may reach the equilibrium temperatures only for case HOT 1.
- The case HOT 3 induces the highest nodal temperature on the satellite being the Sun normal with respect to (one of) the SA, whose corresponding node has the highest absorptivity. Concerning Node 1, where batteries are located, it is within the (margined) thermal envelope.
- In the case HOT 1 the high emissivity of the reflector in the node 1 causes its temperature to exit slightly from the margined range.
- Some devices' needs has been inevitably neglected. The thermal limits imposed by the Star Trackers are overcome: this is the consequence of having assumed for nodes 3 and 4 the absorptivity and emissivity value of the SA. Hence their temperature is more representative of the SA, given also their larger area. A more detailed analysis, accounting for the different coating of the ST (likely MLI) may be necessary to assess the real instrument temperature. Indeed the adopted model is not able to accurately represent the peculiar shape of CryoSat's nose in which the ST are mounted.
- For both the cases HOT 1 and Dynamic the temperature of node 1 is slightly below the defined range. This may indicate two things: the need for an active heating system to restore it and the fact that the model missed details due to its approximation. From [4] the presence of heaters can be acknowledged. A power of 25 W can be assumed for the heaters, assuming that they are used to heat only specific items, such as the batteries, whose thermal behaviour cannot be determined with sufficient resolution with this model. The allocated power is in line with the statistics of 5% of the total power available, indeed it represents the 7.3% after the application of the 25% margin; the total is estimated as 31.25 W.
- Highly conductive straps could be present in the real system to reduce the temperature difference among the nodes, helping the SA to maintain good performances and the electronics to stay above the minimum temperature.
- The Dynamic analysis was conducted in a conservative way to show the worst condition in term of thermal stability. The situation considered is the one with null  $\beta$  angle. It corresponds to the case in which the eclipses are the longest (see Fig. 2.1 for the maximum duration). Furthermore, not having included any transient when switching between dark and light conditions, the thermal excursion is larger than the real one. In particular, the high temperature excursion of the side and top nodes may induce some problems from the structural view point. For what concerns the bottom (node 1), its temperature variation is contained within 6°C/Orbit and is, because of this, deemed sustainable by the electronic components associated. The simplified model so far used did not allow to quantify the thermal variations experienced by the structural supports of

SIRAL antennas, which are known to require high thermal stability. That may be achieved through a better conduction with other surfaces and a dedicated thermal insulation.

The results so far reported and discussed are valid for a given set of materials, assumed to cover each node. Their optical properties are here reported:

	$\alpha$	$\varepsilon$
<b>Node 1</b>	0.217	0.299
<b>Node 2</b>	0.23	0.24
<b>Node 3</b>	0.82	0.82
<b>Node 4</b>	0.82	0.82
<b>Node 5</b>	0.23	0.24

**Table 3.27:** Nodes' external optical properties

They have been determined by means of a trial and error approach, guided by the knowledge that the parameters of the SA are mostly constant across the different types of panels, the radiators data are easily retrievable, and that most of the satellite is covered with MLI. The latter was assumed, given the scarce literature available, to be a kind of Aluminized Kapton because of its appearance. At the first iterations values of  $\alpha = 0.4$  and  $\varepsilon = 0.6$ , standard ones for such materials, have been taken but proved to be unsatisfactory. An  $\alpha/\varepsilon \approx 1$  was deemed necessary. The final values, seen on the previous table 3.27 for nodes 2 and 5, were found in [29] for a particular kind of Aluminized Kapton. From an AO resistance point of view an Aluminized Teflon MLI would have been better but it would have had a too low  $\alpha/\varepsilon$  ratio. The results of the first analysis are reported in the Appendix 3.13 as justification. Moreover, the properties of node 1 have been obtained considering the weighted average on the areas of the already mentioned MLI and of a radiator with  $\alpha = 0.1$  and  $\varepsilon = 0.83$ , the latter covering 10% of the bottom area, its optical properties were selected since average values for standard solar reflectors. Finally given the lack of data, the emissivity of the internal sides of the nodes was put equal to 0.15, i.e. as if the internal surfaces were coated with polished aluminum.

## 3.6 Configuration

The final section of this report will address Cryosat's configuration. The different subsystems positioning will be critically discussed and an estimation of the mass budget will be presented.

### 3.6.1 System Positioning

The satellite platform is characterized by an almost rectangular base shape, above which two solar arrays are mounted, giving the assembly its characteristic tent shape. The cross section of the satellite was kept as small as possible to reduce drag and avoid size conflict with the launcher's fairing (see Fig. A.2). The main structural element of the platform is a rectangular pipe which runs from the rear to the aft of the main structure. Inside it some components, such as on-board electronics, the tank and the reaction control subsystem have been placed. Other instruments like the magnetotorquers have been instead attached to its outer surface. The nadir-pointing plate of the platform is a separate element and the nose part of the satellite as well is a further structurally distinct piece. Finally, the interface to the launcher is made possible by exploiting four mounting points on the rear panel. The structural element are made of aluminum face honeycomb material.

The specific positioning of the internal components inside the platform have been selected by following a few simple guidelines:

- The electronic components have to be located where the excess heat could be easily dissipated (bottom surface and near the nose radiator).

- SIRAL electronics have to be positioned near the antennae to reduce the waveguide length to save mass and signal attenuation
- The centre of gravity (COG) of the satellite is to be fixed or at least its shift has to be predictable for duration of the mission.

These rules found application in the system positioning choices presented in the next figures:

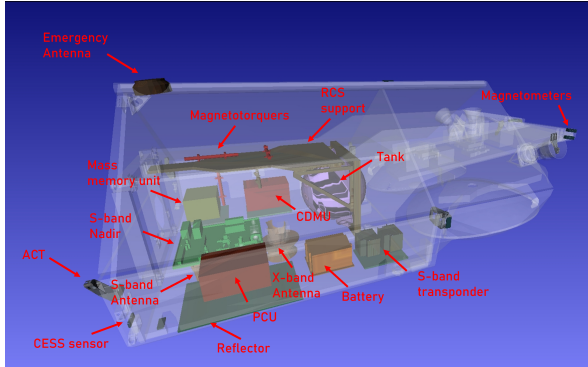


**Fig. 3.15:** CryoSat internal view of its systems elements [1]

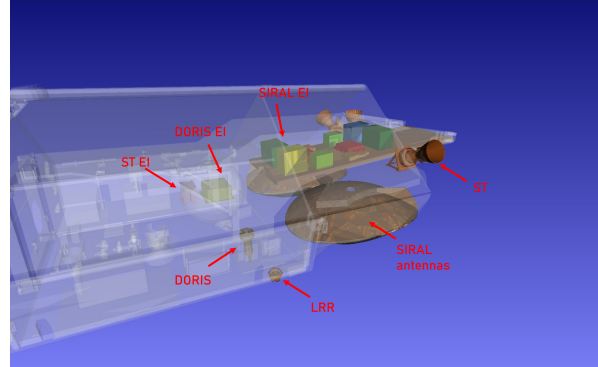


**Fig. 3.16:** CryoSat internal view of its payload and ST [1]

As extensively mentioned, the lower surface of the satellite is permanently Earth facing, even when in safe mode. Because of this, due to the possibility to use the bottom surface to radiate excess heat towards the Earth most of the electronic component have been located there, confirming the considerations made in the thermal analysis. Moreover also the ST electronic interface is located there, this is clearly motivated, besides space reasons, by the high temperatures reached by the top surface of the satellite. For obvious reasons all the equipment needed to communicate with ground was positioned there as well (this includes also the DORIS receiver and the LRR). The only non Earth-facing antenna is the one positioned on the top, between the two SA for emergency use and beacon signal generation after the release.

The RCS support, attached to the central structure serves the purpose to host the piping and valves of the system and is built in aluminium faced honeycomb. The tanks is indeed in the approximate centre of the satellite, where the COG is located: being the propellant consumption the only expected cause of mass variation, this guarantees the COG to stay fixed.

One additional point to be disclosed regards the battery: from the figure it can be seen that it does not sit directly on top of a radiator, hence its heat dissipation is not as high as the one of the PCU. This suggests that keeping it above its minimum temperature was not trivial, as seen with the thermal analysis reported in the previous chapter of this report. This choice, together with the use of strategically located heaters was capable of maintain the battery within its strict operative temperature range.

The CESS sensors distributed locations can be seen as well and confirms its spherical FOV. Concerning the magnetometers they have been positioned as usual far from the electronic components to avoid interference. Usually found on dedicated booms, in the case of CryoSat they have been positioned at the tip of the satellite's nose. In particular they have been located at the opposite side with respect to the magnetotorquers, for the same reason. Moreover, the latter have not been positioned close to the electronics on the bottom surface.

The main payload, SIRAL (both antennae and the electronics), has been accommodated on its dedicated structure which constitutes the nose of the satellite. Beside being a separated structural component it has to answer strict thermal stability and stiffness to minimize the errors induced to SIRAL's measurements. In addition to the payload itself this element also hosts a thermal radiator and the STs. Concerning the last point, this is beneficial as their measurements are directly translated into SIRAL's frame. The antennae are covered with an MLI which is different

from the one covering the main body, specifically chosen to lower their temperature as any antenna benefits from low temperature. The thermal situation of the ST, covered with the same MLI of the main body, was highlighted in section 3.5.3.

With respect to CryoSat-1, the configuration has been slightly modified: the allocation of the MEMS changed the arrangement of the electronics on the bottom plate, while the need for redundant SIRAL electronics was met by placing them in the nose of the satellite. The addition of this redundant masses required an increase of the structural mass.

The resulting mass distribution made the satellite principal axes not to coincide with the geometrical ones. Moreover, the decision of the nose down attitude to compensate for the gravity gradient torque has been taken because of the need to align the flight direction with the principal axis of inertia. The critical Earth-facing antennas and the LRR had to be tilted with respect to the bottom panel to align their boresights orthogonally to the flight direction (see Fig. A.1); the same was done for the ST.

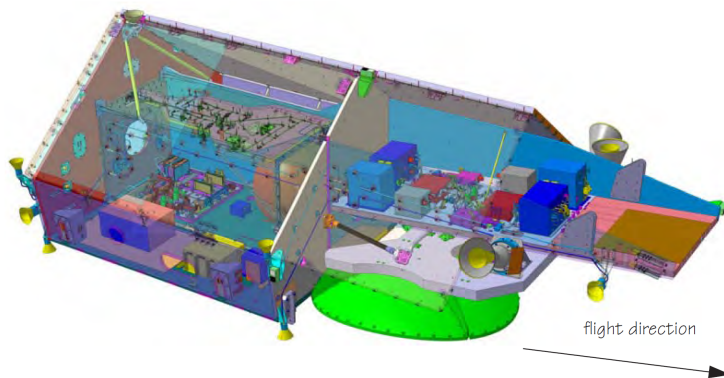


**Fig. 3.17:** Cryosat configuration, internal view

### 3.6.2 Mass budget

Given the lack of data about the components and precise architecture of the satellite the following section will present an estimation, based on statistics, of the mass distribution among the different systems of CryoSat. The only known data are the mass of propellant (36.7 Kg) and payload ( $\sim 90$  Kg), respectively equal to 5% of the wet mass and 13% of the dry mass.

% on the dry mass							
$m_{DRY}$	$m_{P/L}$	$m_{TTMTC}$	$m_{TCS}$	$m_{OBDH}$	$m_{AOCS}$	$m_{EPS}$	$m_{STR}$
687.9 Kg	13.5	1 ÷ 3	1 ÷ 3	2 ÷ 9	6 ÷ 13	19 ÷ 28	26 ÷ 34

**Table 3.28:** Statistical Mass Distribution Estimation

For the identification of the ranges presented in the table 3.28 [30] was consulted. In particular the selected values represent the minimum and maximum reported values relative to satellites whose nominal orbit is the closest to CryoSat's. By analyzing the statistics it was possible to infer that CryoSat's case is an anomaly because of its low payload dry mass fraction. The reasons for this could have been:

- A less efficient structural design than the average satellite.
- A necessarily heavier structure due to the need to accommodate SIRAL's front end in a highly sturdy secondary structure.
- Shortcomings in the production phase which lead towards the allocation of more mass than initially expected.

# A | CryoSat's Configuration

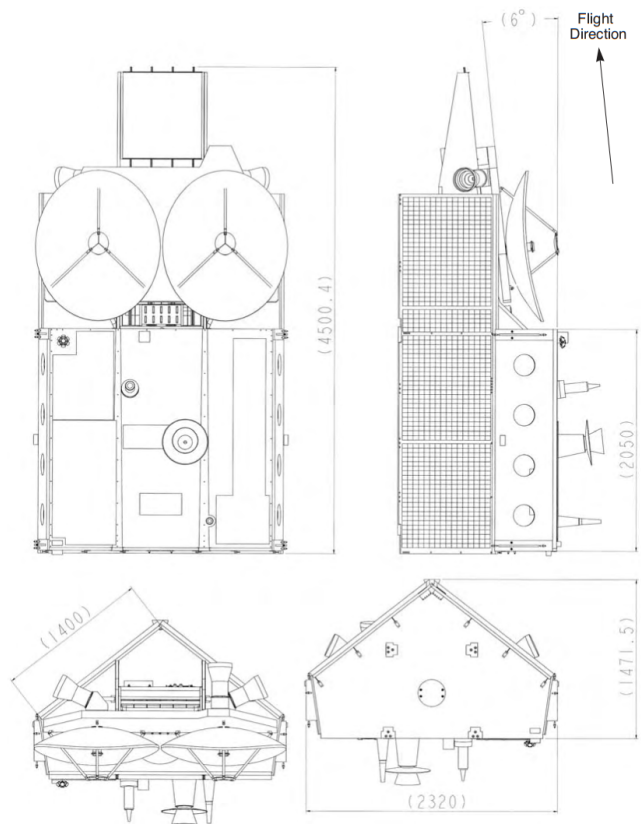


**Fig. A.1:** CryoSat's dimensions

The fitting of the satellite into the launcher's fairing can be observed in the following figure. It can be noticed how the satellite body is not in close proximity to the launcher's internal walls to fit within the dynamic envelope of the payload bay.

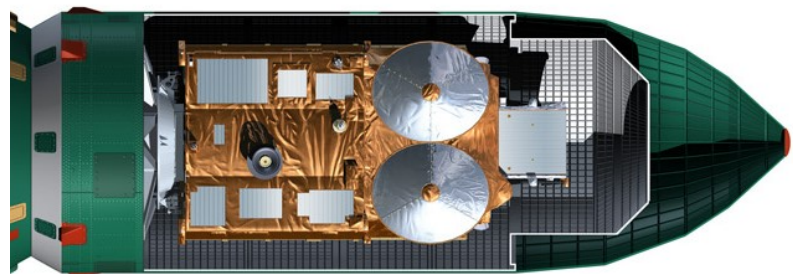


**Fig. A.2:** CryoSat inside the fairing

# B | Launcher

The launcher is a three-stage vehicle converted SS-18 intercontinental ballistic missile. The first and second stages are original SS-18 stages, used without any modification. The third stage is a modified standard SS-18 third stage equipped with a liquid propellant, two-mode propulsion unit that operates based on a 'drag' scheme in which it flies backwards, dragging the satellite behind it to ensure the most accurate orbit injection. The overall length is 34 m, and the overall diameter is 3 m. The lift-off mass of the rocket is 211 t. It is launched from a silo, being expelled like a mortar round with a charge of black powder, before the main engine ignition some 30 m above the ground. The cost per launch was 29M\$.

The choice of this launcher lies in its high reliability index, equal to 0.97, and in its characteristics in terms of accuracy reported in Tab.B.1. They are referred to LEO orbits with high inclination such as that required by the CryoSat satellite.

Parameter	$h = 300\text{km}, i = 98^\circ$	$h = 600\text{km}, i = 98^\circ$	$h = 900\text{km}, i = 98^\circ$
Altitude [km]	$\pm 4.0$	$\pm 5.5$	$\pm 10.0$
Period of revolution [s]	$\pm 3.0$	$\pm 4.0$	$\pm 6.5$
Inclination [deg]	$\pm 0.040$	$\pm 0.045$	$\pm 0.050$
RAAN [deg]	$\pm 0.050$	$\pm 0.060$	$\pm 0.070$

Table B.1: Spacecraft Injection Accuracy for circular orbit of Dnepr Launcher

In Fig.B.1 are shown the ConOps of the launcher.

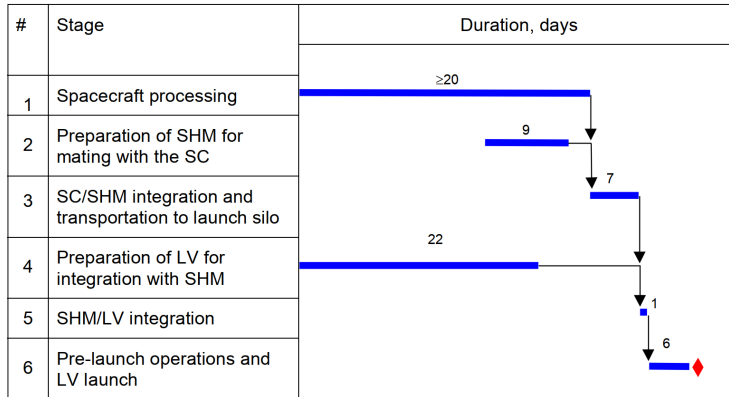


Fig. B.1: Launcher Con-ops

From [31] the maximum quasi-static acceleration values at the interface between satellite and launch vehicle (LV) for the different phases of the mission are found:

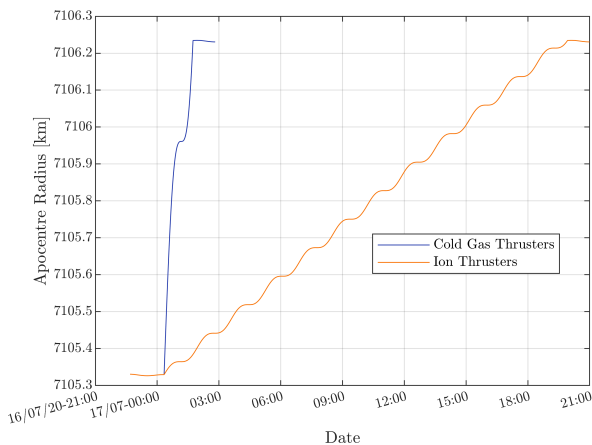
Load Source	Acceleration [g]	
	Longitudinal	Lateral
LV movement inside TLC	$2.5 \pm 0.7$	$\pm 0.3$
After LV exit from TLC	$\pm 1$	$\pm 0.8$
1 <sup>st</sup> Stage burn:		
Maximum dynamic head	$3.0 \pm 0.5$	$0.5 \pm 0.5$
Maximum longitudinal acceleration	$7.5 \pm 0.5$	$0.1 \pm 0.5$
2 <sup>nd</sup> Stage Burn		
Maximum longitudinal acceleration	$7.8 \pm 0.5$	0.2
3 <sup>rd</sup> Stage Burn	$-0.3 \div -0.5$	0.25

Table B.2: Maximum Launcher Acceleration

# C | Engine Comparison

In this section the results of the analysis of a manoeuvre are presented. As already mentioned, in 2020 CryoSat manoeuvred to provide measurement synchronized with ICESat2. This manoeuvre, which is one of the few manoeuvre of orbit change, modified the size of the nominal orbit and increased the apogee radius by 900 meters. It was selected for the analysis and modelled with the aid of GMAT. A comparison with an hypothetical ion grid thruster was performed. Being interested only in the nominal cost of the manoeuvre, no disturbances were accounted for. The manoeuvre starting date considered is the 17<sup>th</sup> July 2020. The mass of the satellite, dry and wet at this date were retrieved from the DORIS service dedicated website.

The manoeuvre was considered to start at the pericentre of the orbit, after the end of the manoeuvre the orbit is propagated until the apocentre, now matching the required one of 7106.23km. The Ion thruster considered for the comparison has the following notable data: Thrust 5mN, Impulse 1900s. The cold gas thruster system was considered to operate with a thrust equal to 80mN (i.e. with two nozzles operating).



**Fig. C.1:** Apocentre radius variation.

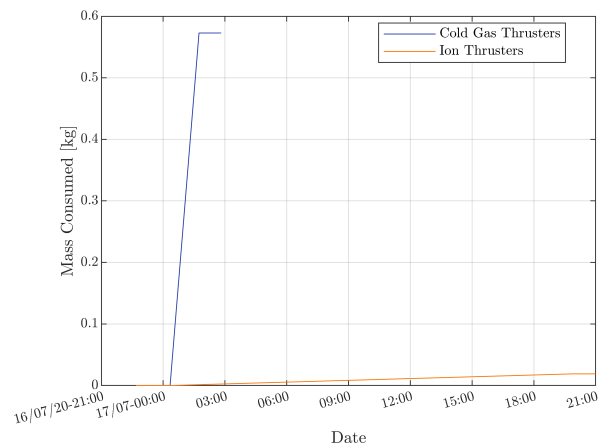


**Fig. C.2:** Propellant mass consumption.

From Fig. C.1 one can see how the solution adopted for CryoSat design allowed to take less time to perform the change than the alternative ion thruster, indeed the adopted solution required a continuous firing of 5060s, the alternative one more than 70500s. Fig. C.2 instead highlights the main advantage of the alternative solution: a far lower propellant mass consumption. Once the mass variation is obtained the associated  $\Delta V$  budget can be estimated equal to 0.564 m/s. Being part of the extended life program it is highly probable that this was not accounted for when defining the total velocity budget of the mission.

Finally, another important detail shall be considered: the power required. The alternative was indeed selected in virtue of its low power requirement: 145W. Such power, however, required for such long time is bound to need way more energy than the one needed to operate the cold gas thruster system, which can be assumed to be close to 20 W (as only two OCT nozzles are considered operative). Moreover, given the limited power availability the ion thrust solution might in principle need to be paused when in eclipse (even though this is not an issue as the manoeuvre could be scheduled for an epoch without eclipses). This justifies the selection made by the designers.

# D | Thermal Analysis

## D.1 Results of refined MLI selection

These are the plots whose data were used for the definition of the table 3.13.

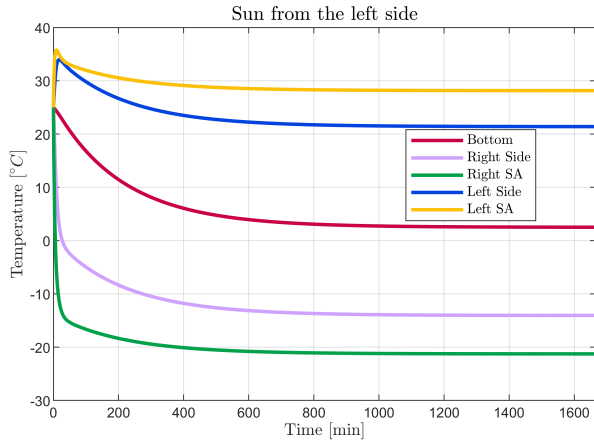


**Fig. D.1:** Hot case 1: Sun direction along y-axis.

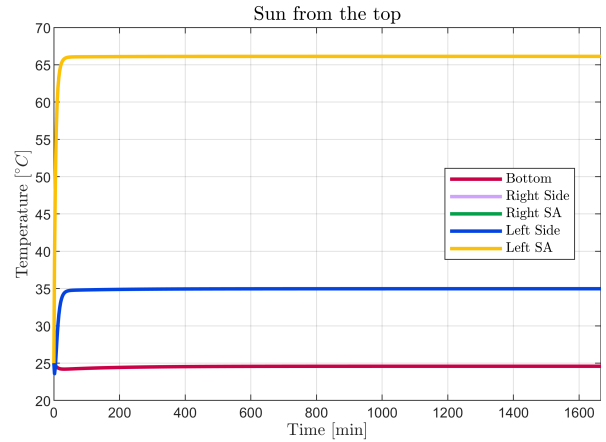


**Fig. D.2:** Hot case 2: Sun direction along z-axis

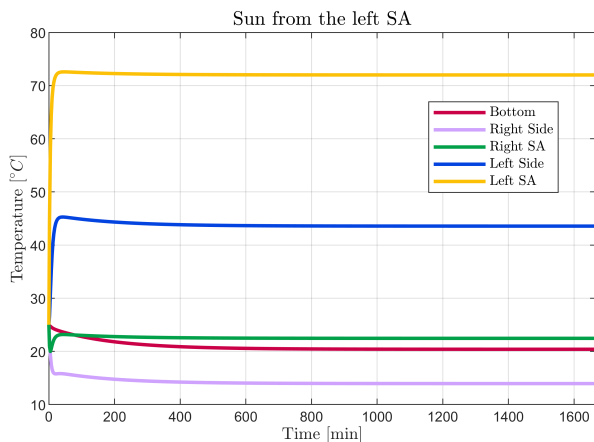


**Fig. D.3:** Hot case 3: Sun direction normal to the SA

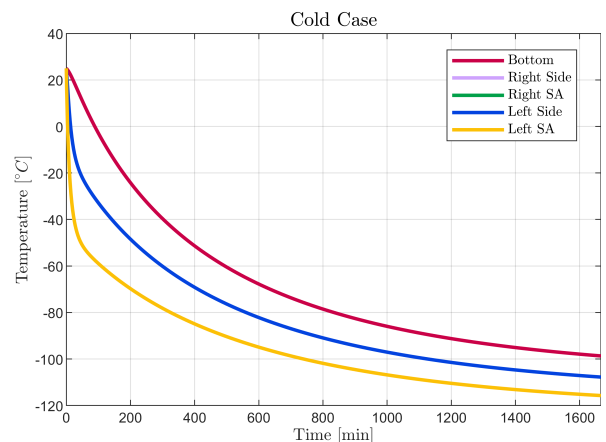


**Fig. D.4:** Cold case: Eclipse

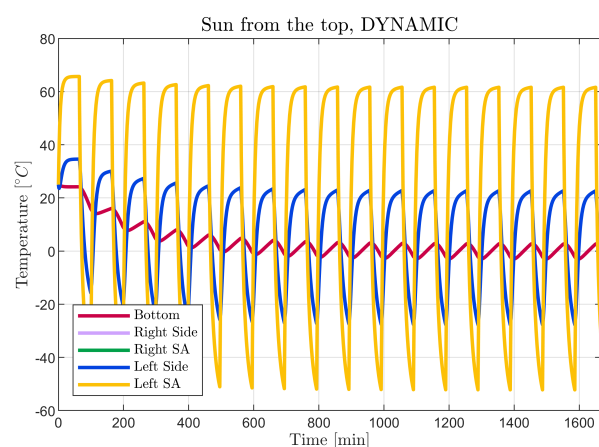


**Fig. D.5:** Dynamic Thermal Study

## D.2 Results of initial MLI selection

These plots represent the results for a generic Aluminized Kapton MLI.

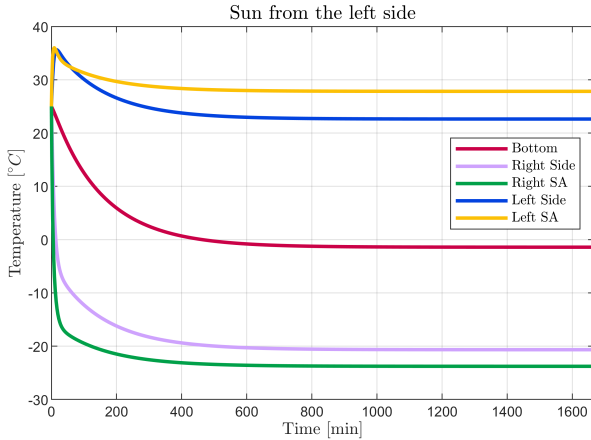


**Fig. D.6:** Hot case 1 (general MLI): Sun direction along y-axis.

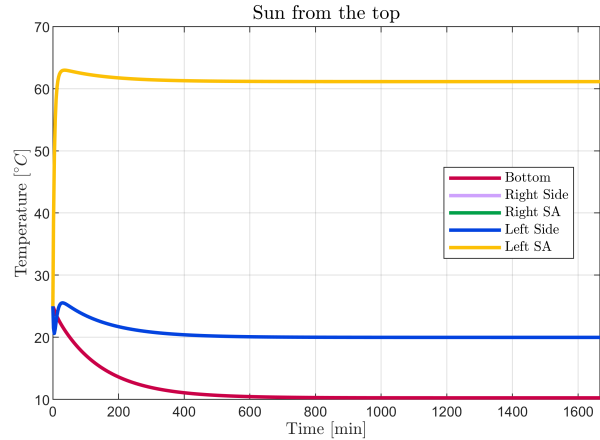


**Fig. D.7:** Hot case 2 (general MLI): Sun direction along z-axis

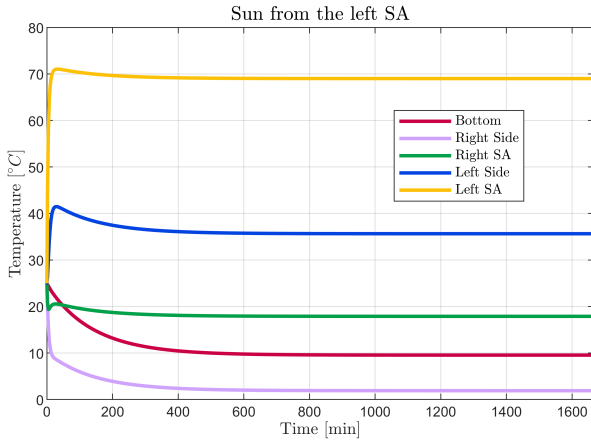


**Fig. D.8:** Hot case 3 (general MLI): Sun direction normal to the SA

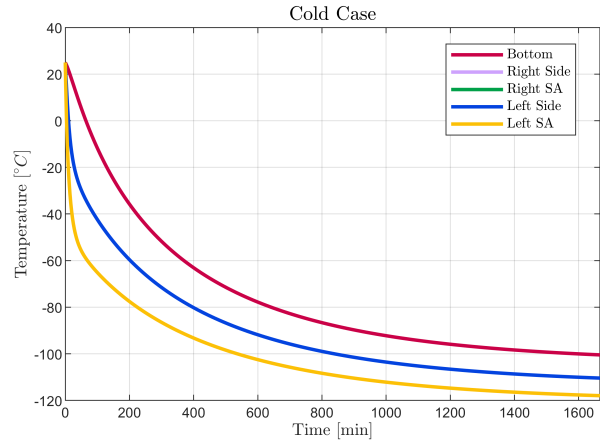


**Fig. D.9:** Cold case (general MLI): Eclipse

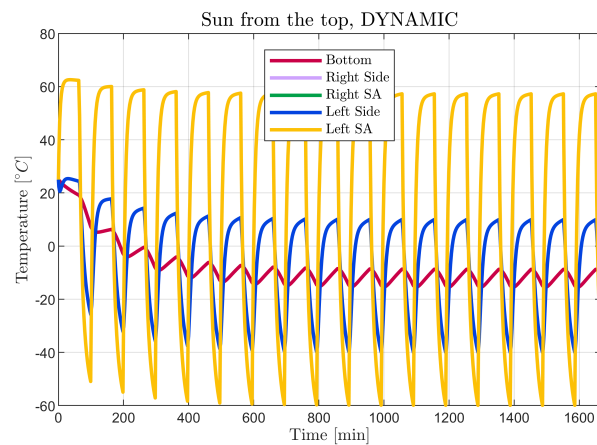


**Fig. D.10:** Dynamic Thermal Study (general MLI)

As the figures show, the selection of a generic Aluminized Kapton would not allow the node 1 (bottom) to be kept inside the acceptable range defined before. Thus this specific material has been discarded.

# E | On-Board Data Handling

The On-board-data-handling (OBDH) subsystem is in charge of processing, storing and transmitting all the data of the electronics units on board. The nature of the data could be scientific, when generated by the payload, or technical, when generated by the other subsystems present on board. The main purpose of the CryoSat satellite is to download the scientific data produced by the payload, this highlight the need to store large quantities of data until a visibility of the Ground Station is granted for the data transfer. Also, the OBDH subsystem is in charge to handle the telemetry and health status data of the other subsystems present on-board to apply a control over the whole spacecraft with a certain degree of autonomy.

In this section, the computer performances will be estimated to justify the real baseline architecture and the hardware through an iterative process and to understand how it contributes to the overall mass and power budgets of the spacecraft.

## E.1 Functionalities

- **F.12.1** Store all the data until their download
- **F.12.2** Control and distribute commands to the systems present on board
- **F.12.3** Process the data coming from the sensors present on board
- **F.3.7** Prepare the data for transmission

## E.2 Baseline architecture

The block diagram architecture of the subsystem is reported in Figure E.1.

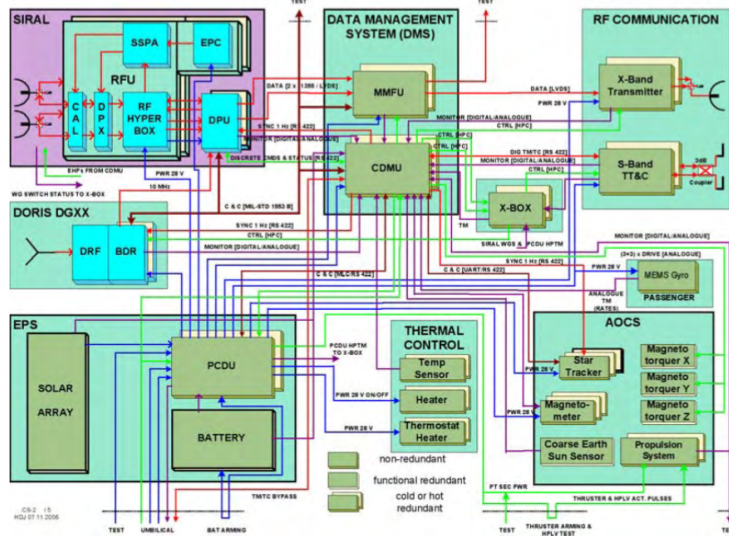


**Fig. E.1:** Block diagram of the major elements of CryoSat OBDH architecture [4]

The baseline architecture refers to the block diagram of the OBDH subsystem: it is a method to show how the different subsystems interact between each other to achieve the mission objectives. The choice of the architecture is strictly correlated to the performance requirements of the mission and in particular is strongly affected by the way in which the processing instructions shall be executed.

It is possible to notice in Figure E.1 that CryoSat is equipped with a centralized architecture, a

reliable system since possible failures can affect only one line. This scheme works best when all the systems on board are well defined and directly connected to the central unit but the wiring can become very complex.

The Central Data and Management Unit (CDMU) is the core of the architecture, it interfaces to all the other subsystems: it receives from them the health-status data and provide commands. The most complex units such as the payload ones (SIRAL and DORIS) are connected via MIL-Bus-1553 while the other units are connected through relatively simple serial links.

The CDMU runs different tasks concurrently:

- **Autonomy:** For the CryoSat satellite a simple level of autonomy is considered, the CDMU decodes and interprets commands from the Ground Segment. These commands can be passed for the immediate execution to the units or, if they're time-tagged, they can be later executed by controlling the master timeline. Monitors and fault detection mechanisms are implemented to identify and correct failures and adverse conditions in the on-board equipment. Those data can be later downloaded to the ground for diagnosis and commanding.
- **ADCS management:** The attitude sensor software handles data from various sensors, compensate misalignments and biases and transforms data into internal coordinates to be sent to the actuators. The Attitude determination and control category shall also be capable to perform kinematic integration, to estimate the current attitude by integrating sensed body rates, error determination, to understand how far the spacecraft's orientation is with respect to the desired one, and precession control.
- **EPS management:** The computer controls battery charge and discharge and monitors the power bus in order to ensure that every component on board receives the correct amount of power.
- **TCS management:** The computer shall be capable to monitor and control the temperatures throughout the whole spacecraft to ensure that the operational temperature of each component of the spacecraft is maintained during the whole mission.
- **TTMTC management:** This function is used to interface the OBDH s/s with the telecommunication one, it includes processing external commands and collecting internal data for transmission to an external source. The S-band Transceiver, together with S-band antennas, is the physical means by which the CDMU and its telecommand decoder interface to the Ground Segment.
- **Payload management:** The computer controls the different operational modes of the payloads on-board in different phases of the mission. The MMFU includes a fast data formatter which formats and frames the data, assigning it to a number of virtual data channels, and applying Reed-Solomon error correction codes. These data frames are collected and stored until the first transfer window when they will be transferred to the X-band downlink sub-system.
- **RTOS (Real-time operating system):** This section comprehends the executive, the code that manages and schedules the application software and the operating-system functions, the Run-time kernel, which stores, optimizes and packs the data, the I/O handler, which controls the data that flows in and from the processors along with a Built-In Test and Diagnostic and Math Utilities functions.

### E.3 OC performance estimation

Through the OC performance estimation (with a statistical analysis) it is possible to specify the processing tasks and determine the data requirements to size the RAM, the ROM and the data storage architecture of a spacecraft. The software size is calculated in terms of words of memory (Kwords) and million of instructions per seconds (MIPS), basing the numerical values on similarity

with other mission, as reported in Wertz and Brown book [30]. Starting from these set of values, their are changed accordingly to the frequencies required for each task.

The result coming from the analysis presented in Table E.1 will be used to justify the selection of the processor equipped in CryoSat.

Function	#	Code (Kwords)	Data (Kwords)	Throughput (KIPS)	Frequency (Hz)
<b>ADCS</b>					
Sun Sensor	1	2	0.1	1	1
Star Tracker	3	2	15	2	1
Magnetometers	3	0.2	0.1	1	2
Magnetotorquers	3	1	0.2	3	3
Thruster control	16	0.6	0.4	1.2	2
Kinematic integration	1	2	0.2	15	10
Error determination	1	1	0.1	12	10
Precession control	1	3.3	1.5	30	10
Orbit propagation	1	13	4	20	1
Ephemeris propagation	1	2	0.3	2	1
<b>Autonomy</b>					
Simple autonomy	1	2	1	1	1
<b>Fault detection</b>					
Monitors	1	4	1	15	5
Fault correction	1	2	10	5	5
<b>Other functions</b>					
Solar array control	1	9	1.05	-	2.5
Power management	1	1.2	0.5	5	1
Thermal control	1	0.8	1.5	3	0.1
<b>Communication</b>					
Antennas	1	1.2	1.4	-	40
Command	1	1	4	7	10
Telemetry	1	1	2.5	3	10
Payload*	1	1	100	100	-
<b>RTOS</b>					
Executive	1	3.5	2	60	-
Run-time-kernel	1	8	4	-	-
I/O device handlers	1	2	0.7	40	-
Built-in test and diagnostic	1	0.7	0.4	0.5	-
Math utilities	1	1.2	0.2	-	-
<b>Subtotal</b>		0.166 MB	0.387 MB	0.357 MIPS	
Margin		400%	400%	400%	
<b>Total</b>		<b>0.664 MB</b>	<b>1.546 MB</b>	<b>1.427 MIPS</b>	

\*Payload values have been estimated and margined based on the FireSat example in [30]

**Table E.1:** CryoSat OC performance estimation

The values reported in Table E.1, represents the first evaluation of the computer performance for a Phase A analysis, for this reason a margin of 400% has been considered to take into account possible changes in future phases of the design. Also, this performance estimation has been carried out by considering the WCC (Worst Case Condition) which occurs when all the functions are active.

The RAM has been calculated by summing the data and the code that have been executed while the ROM has been evaluated considering the SLOC of the system, associated to the code, excluding the run-time kernel. The results are reported in Table E.2.

RAM [MB]	ROM [MB]	MIPS
2.211	10.353	1.427

**Table E.2:** OC results

## E.4 Hardware

The CryoSat satellite is equipped with two redundant ERC32 TSC695F(L) SPARC V7 processors [30], 4 MB of RAM and 16 MB of ROM. This processor is capable to provide 20 MIPS and it has a large flight heritage, given the results reported in Table E.2, the hardware equipped in CryoSat is capable to sustain the performances requested for the whole duration of the mission. The specifications are reported below in Table (E.3).

Throughput	20 MIPS
TRL	9
Rad Hardness	300 krad
Weight	0.1 Kg
Power consumption	1 W

**Table E.3:** ERC32 TSC695F(L) SPARC V7 processor specifications [12]

# F | Requirements

## F.1 Mission Requirements

- **R-MIS-001** The launcher shall be capable to inject the s/c in the final orbit.
- **R-MIS-002** The s/c orbit shall be highly inclined to be capable to make measurements at high latitudes.
- **R-MIS-003** The orbit of the s/c shall be retrograde to provide higher frequencies of updates.
- **R-MIS-004** The s/c shall have an orbit which is capable to offer high-density coverage over the Polar Regions and sufficient measurements down to the south of Greenland.
- **R-MIS-005** The s/c shall be capable to acquire scientific data regarding the Earth's cryosphere.
- **R-MIS-006** The s/c shall be capable to communicate the scientific data to the ground.
- **R-MIS-007** The s/c shall be capable to sustain at least the nominal mission duration.
- **R-MIS-008** The mission shall be controlled from ESA/ESOC facility.
- **R-MIS-009** The data shall be distributed to the final users by ESA/ESRIN facility.
- **R-MIS-010** The s/c shall be capable to conduct the scientific operations regardless of the eclipse phases.
- **R-MIS-011** The orbit altitude shall be designed accordingly to the scientific requirements and instrument capabilities.
- **R-MIS-012** The data coming from different instruments shall be merged in order to obtain meaningful results.
- **R-MIS-013** The s/c shall be equipped with a system for orbital maintenance.
- **R-MIS-013** The mission shall last at least 3.5 years.

## F.2 Environmental Requirements

- **R-ENV-001** The embrittlement of thermal protection materials shall be limited.
- **R-ENV-002** The s/c shall be capable to withstand the external magnetic field encountered during the mission, in order to avoid disturbances in the instrumentation.
- **R-ENV-003** The s/c shall be capable to withstand the flux of ionized particles.
- **R-ENV-004** The s/c coating shall withstand the erosion due to AO caused during the designed life duration.
- **R-ENV-005** The s/c shall be capable to withstand the radiation dose experienced during the designed life mission.
- **R-ENV-006** Sensitive components shall be positioned far from contamination sources.
- **R-ENV-007** Resin based sealants and adhesives should be avoided.
- **R-ENV-008** Double wall shielding should be adopted to protect important components.
- **R-ENV-009** The s/c should use sandwich panels for the lateral faces.
- **R-ENV-010** The s/c should be able to turn off the payload in case of severe magnetic storms.

### F.3 Design Requirements

- **R-DES-001** No failure of single unit component shall lead to a failure of another component/subsystem.
- **R-DES-002** All the adopted margins shall comply with the ESA standard margin philosophy.

### F.4 Telecommunication System

- **R-DES-TTMTTC-001** The TTMTTC s/s shall comply with the ESA telecommunication standards.
- **R-DES-TTMTTC-002** The s/c shall interface with the ESA network Ground Stations.
- **R-FUN-TTMTTC-003** The link shall be maintained during all safety critical mission phases.
- **R-FUN-TTMTTC-004** The TTMTTC s/s shall be capable to provide a real-time link for monitoring and control the system during all mission phases.
- **R-FUN-TTMTTC-005** The TTMTTC s/s shall satisfy the uplink and downlink request for data transmission during all mission phases.
- **R-MIS-TTMTTC-006** The TTMTTC s/s shall be capable to download all the data produced by the payload.
- **R-FUN-TTMTTC-007** The TTMTTC s/s shall be capable to download the telemetry of the s/c to the ground and to upload commands from the Ground segment.
- **R-DES-TTMTTC-008** CryoSat shall be equipped with an X-band architecture to download the payload data.
- **R-DES-TTMTTC-009** CryoSat shall be equipped with an S-band architecture to download the telemetry of the s/c and to receive commands from the Ground Stations.
- **R-FUN-TTMTTC-010** The TTMTTC subsystem for both satellites shall enable spacecraft's mode changes through ground commands.
- **R-FUN-TTMTTC-011** CryoSat shall be capable to send to the ground station its telemetry during the LEOP phase whatever its attitude is.
- **R-FUN-TTMTTC-012** In case of operations failures the CryoSat satellite shall provide data regarding the problem encountered.
- **R-DES-TTMTTC-013** CryoSat shall be equipped at least with an omnidirectional antenna to be capable to communicate its trajectory and attitude whatever its attitude is.
- **R-DES-TTMTTC-014** - CryoSat shall be equipped at least with a high-gain antenna to communicate scientific data collected during the operations.

### F.5 Propulsion System

- **R-FUN-PRO-001** The Propulsion system shall allow to perform orbital manoeuvres.
- **R-FUN-PRO-002** The Propulsion system should provide auxiliary attitude control.
- **R-DES-PRO-003** The propellant shall be storable.
- **R-DES-PRO-004** The propellant shall be inert.
- **R-OP-PRO-005** The pressure before the nozzle shall be fixed.
- **R-DES-PRO-006** The architecture of the system shall be robust against nozzle failure.
- **R-DES-PRO-007** The propulsion system shall have redundant thrusters.

- **P-FUN-PRO-008** The propulsion system should be able to operate when in eclipse.
- **R-OP-PRO-009** The system shall be restartable even after months.
- **R-OP-PRO-010** The tank shall contain sufficient propellant for the established lifetime.
- **R-FUN-PRO-011** The s/c shall be capable to perform collision avoidance manoeuvres.
- **R-PRO-DES-012** The tank shall be sized for a burst pressure equal to 1.5 times the nominal maximum pressure of the propellant.

## F.6 Attitude Determination and Control System

- **R-FUN-ADCS-001** The nominal attitude of the satellite shall be nadir pointing.
- **R-PERF-ADCS-002** The system shall guarantee a pointing accuracy better than  $0.2^\circ$  when in fine pointing mode.
- **R-PERF-ADCS-003** The system shall guarantee a pointing knowledge more accurate than  $35''$  when in fine pointing mode.
- **R-PERF-ADCS-004** The system shall guarantee a pointing stability better than  $0.005^\circ$  over 0.5s when in fine pointing mode.
- **R-PERF-ADCS-005** The system shall guarantee a pointing accuracy better than  $15^\circ$  when in coarse pointing mode.
- **R-PERF-ADCS-006** The system shall guarantee a pointing knowledge more accurate than  $6^\circ$  when in coarse pointing mode.
- **R-PERF-ADCS-007** The system shall damp initial rates of  $3^\circ/\text{s}$  to below  $0.1^\circ/\text{s}$  in less than 75 minutes.
- **R-OP-ADCS-008** When in orbit control mode eventual thrust misalignment shall be compensated.
- **R-FUN-ADCS-009** The system shall transition autonomously between the selected pointing modes.
- **R-DES-ADCS-010** No moving mechanism should be on board.
- **R-OP-ADCS-011** When in safe mode the system shall be put in coarse pointing mode
- **R-DES-ADCS-012** The system shall avoid single point failures.
- **R-DES-ADCS-013** The sensor network shall comprise multiple sensors in a hot redundant scheme.
- **R-PERF-ADCS-014** The system shall reconstruct the attitude even from a lost in space condition.
- **R-PERF-ADCS-015** The actuator shall be able to provide at least  $3 \times 10^{-4} \text{ Nm}$  along each axis to compensate the disturbances.

## F.7 Electric Power System

- **R-FUN-EPS-001** The system shall provide the required power to other subsystems and payload for each mode and for each mission phase.
- **R-FUN-EPS-002** The Electric power system must work for the entire mission life.
- **R-FUN-EPS-003** The system shall withstand both average and peak power demand.
- **R-OP-EPS-004** The system shall work in the operational range of temperatures.
- **R-MIS-EPS-005** The Electric power system shall be able to work also in absence of sunlight.

- **R-DES-EPS-006** The Electric power system shall be able to withstand failures.
- **R-FUN-EPS-007** The Electric power system shall be able to supply power during off-nominal conditions and peak power demands.
- **R-FUN-EPS-008** The Electric power system shall avoid damages to the instrumentation in case of malfunction.
- **R-FUN-EPS-009** The Electric power system shall not produce any undesired interference on the other components.
- **R-FUN-EPS-010** The EPS shall regulate/control the electrical power depending on the loads, on the mission profile and on the source degradation.
- **R-DES-EPS-011** The EPS shall contain a secondary energy storing source for peak power requests and for phases in which the primary energy source is not available.
- **R-DES-EPS-012** CryoSat shall use solar arrays as primary power source covered with multiple junction cells.
- **R-DES-EPS-013** CryoSat shall use Li-ion batteries as secondary power source.

## F.8 Thermal Control System

- **R-FUN-TCS-001** The TCS shall guarantee that the temperatures inside the satellite never fall outside the strictest operative range when such device is being used actively.
- **R-FUN-TCS-002** The TCS shall guarantee that the temperatures inside the satellite never fall outside the non-operative range when devices are not being used actively.
- **R-FUN-TCS-003** The TCS shall prevent the temperature to fall outside the survivability range under any circumstance.
- **R-PERF-TCS-004** The coating materials degradation shall guarantee the respect of the previous requirement for the nominal mission duration.
- **R-OP-TCS-005** An active system shall be present on board to prevent the most sensitive component temperature to fall below their lower operability threshold.
- **R-DES-TCS-005** Heaters should be applied to those equipment which need to be warm up during eclipses.

## F.9 On Board Data Handling

- **R-FUN-OBDH-001** The OBDH subsystem shall be capable to store all the data until the download phase during a transfer window.
- **R-FUN-OBDH-002** The OBDH subsystem shall be capable to control and distribute commands to the other subsystems present on-board.
- **R-DES-OBDH-003** The OBDH subsystem shall be capable to withstand the total radiation dose encountered during the mission.
- **R-FUN-OBDH-004** The OBDH subsystem shall process the data coming from the sensors of the other subsystems present on board.
- **R-DES-OBDH-005** CryoSat shall be equipped with a centralized architecture.

## F.10 Configuration

- **R-DES-CONF-001** A launch mass margin of 20% shall be considered according to ESA philosophy.

- **R-DES-CONF-002** The spacecraft system shall accommodate all necessary equipment and subsystems, including mass and volume margins and compatible with launch windows.
- **R-DES-CONF-004** A design-to-cost and risk minimization mission design approach shall be followed.
- **R-DES-CONF-005** The design of the sampling spacecraft and ERC shall be robust against damage due to debris.
- **R-FUN-CONF-006** The spacecraft structure shall support the launch environment.
- **R-CONF-FUN-007** The spacecraft structure shall support the mechanical static and dynamic loads encountered during its entire lifetime.
- **R-DES-CONF-008** The structural stiffness shall guarantee fundamental frequencies of the S/C within the requirements of the LV to avoid dynamic coupling.
- **R-DES-CONF-009** Payload tank shall be placed in the CoM of spacecraft.
- **R-DES-CONF-010** Antennas and sensors visibility shall be assessed.
- **R-DES-CONF-011** SIRAL antennas shall be Earth pointing.
- **R-DES-CONF-012** The ST shall be oriented to minimize the possibility of contemporary blinding of 2 sensors due to the sun and the moon.
- **R-DES-CONF-013** The OCT shall be aligned with the s/c centre of mass.

# Bibliography

- [1] ESA. ESA mobile app. [Online]. Available: <https://www.esa.int>
- [2] D. King-Hele, *Satellite orbits in an atmosphere. Theory and applications.* Springer, 1987.
- [3] S. Lemmens and F. Letizia, “Esa’s annual space environment report,” Technical Report GEN-DB-LOG-00288-OPS-SD, ESA Space Debris Office, Tech. Rep., 2020.
- [4] Cryosat mission and data description. [Online]. Available: [https://esamultimedia.esa.int/docs/Cryosat/Mission\\_and\\_Data\\_Descrip.pdf](https://esamultimedia.esa.int/docs/Cryosat/Mission_and_Data_Descrip.pdf)
- [5] I. T. U. (ITU), “Radio regulations article: Volume 1,” 2016.
- [6] ESA. Etrack ground stations. [Online]. Available: [https://www.esa.int/Enabling\\_Support/Operations/ESA\\_Ground\\_Stations/Etrack\\_ground\\_stations](https://www.esa.int/Enabling_Support/Operations/ESA_Ground_Stations/Etrack_ground_stations)
- [7] Sputnix. Sputnix sxc-xtx-01. [Online]. Available: <https://www.satcatalog.com/component/x-band-transmitter-622/>
- [8] ISISPACE. Isinspace s-band transceiver. [Online]. Available: <https://www.satcatalog.com/component/s-band-transceiver/>
- [9] G. P. Sutton and O. Biblarz, *Rocket propulsion elements.* John Wiley & Sons, 2016.
- [10] H. Junginger. The cryosat power system. [Online]. Available: <https://ui.adsabs.harvard.edu/abs/2002ESASP.502....3J/abstract>
- [11] T. Ormston, L. Maleville, V. D. Tran, L. Lucas, K. Van Der Pols, M. Denis, and N. Mardle, “Lithium ion battery management strategies for european space operations centre missions,” in *SpaceOps 2014 Conference*, 2014, p. 1883.
- [12] ATMEL. Erc32 tsc695f(l) sparc v7 processor. [Online]. Available: <http://ww1.microchip.com/downloads/en/devicedoc/doc4118.pdf>
- [13] eoportal directory - cryosat-2. [Online]. Available: <https://directory.eoportal.org/web/eoportal/satellite-missions/c-missions/cryosat-2>
- [14] International doris service. [Online]. Available: <https://ids-doris.org/>
- [15] Precision orbit determination doris. [Online]. Available: <https://www.aviso.altimetry.fr/en/techniques/doris/principle.html>
- [16] Lrr datasheet. [Online]. Available: [https://ilrs.cddis.eosdis.nasa.gov/docs/CRYOSAT\\_LRR\\_01\\_DATA\\_PACKAGE.pdf](https://ilrs.cddis.eosdis.nasa.gov/docs/CRYOSAT_LRR_01_DATA_PACKAGE.pdf)
- [17] General mission analysis tool nasa. [Online]. Available: <https://software.nasa.gov/software/GSC-17177-1>
- [18] Esa space debris mitigation compliance verification guidelines. [Online]. Available: <https://copernicus-masters.com/wp-content/uploads/2017/03/ESSB-HB-U-002-Issue119February20151.pdf>
- [19] T. Parrinello, A. Shepherd, J. Bouffard, S. Badessi, T. Casal, M. Davidson, M. Fornari, E. Maestroni, and M. Scagliola, “Cryosat: Esa’s ice mission—eight years in space,” *Advances in Space Research*, vol. 62, no. 6, pp. 1178–1190, 2018.
- [20] Esa master tool website. [Online]. Available: <https://sdup.esoc.esa.int/master/>

- [21] Spenvis tool suite for environmental analysis. [Online]. Available: <https://www.spenvis.oma.be/>
- [22] MOOG. Cold gas thruster datasheet. [Online]. Available: <https://www.moog.com/products/propulsion-controls/launch-vehicles/cold-gas-thrusters.html>
- [23] P. Smith, S. Edwards, and N. Solway, "Cryosat cold gas system and component development," in *40th AIAA/ASME/SAE/ASEE Joint Propulsion Conference and Exhibit*, 2004, p. 3859.
- [24] T. Usbeck, N. Diske, and S. Schulz, "The cryosat aocs-a cost-efficient design for small earth observation satellites," *Spacecraft Guidance, Navigation and Control Systems*, vol. 516, p. 323, 2003.
- [25] Satsearch. Star tracker he-5as. [Online]. Available: <https://satsearch.co/products/terma-he-5as>
- [26] NASA, "Nasa space vehicle design criteria monograph (guidance and control), spacecraft magnetic torques," *NASA SP-8018, March*, 1969.
- [27] I. D. Service. Mass and gravity centre history. [Online]. Available: <ftp://ftp.ids-doris.org/pub/ids/satellites/cs2mass.txt>
- [28] S. Pessina and S. Kasten-Coors, "In-flight characterisation of cryosat-2 reaction control system," in *22nd International Symposium on Space Flight Dynamics*, 2011.
- [29] J. H. Henninger, *Solar absorptance and thermal emittance of some common spacecraft thermal-control coatings*. National Aeronautics and Space Administration, Scientific and Technical ..., 1984, vol. 1121.
- [30] J. R. Wertz, D. F. Everett, and J. J. Puschell, *Space mission engineering: the new SMAD*. Microcosm Press, 2011.
- [31] Dnepr launcher manual. [Online]. Available: [http://www.kosmotras.ru/en/docs\\_mkk/](http://www.kosmotras.ru/en/docs_mkk/)
- [32] Cryosat's objectives. [Online]. Available: <https://earth.esa.int/eogateway/missions/cryosat/objectives>
- [33] C. NASA, "Us-french jason-1." [Online]. Available: <http://sealevel.jpl.nasa.gov/>